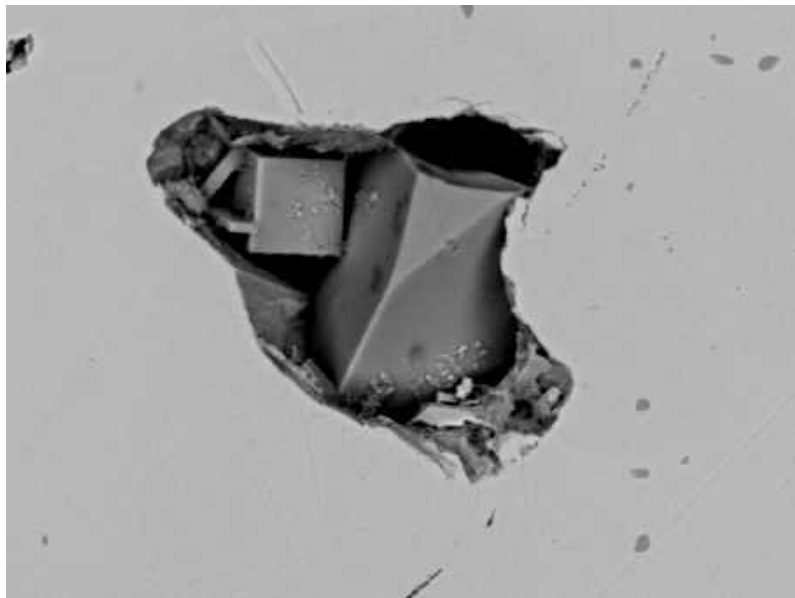


Silver Mineralogy and Modes of Occurrence at the Silver Hart Deposit, South East Yukon.



Michael Ives-Ruyter

Geosciences, master's level (120 credits)
2023

Luleå university of technology
Department of Civil, Environmental and Natural Resources Engineering

[This page intentionally left blank]

Abstract

The Silver Hart property is a high grade silver-lead-zinc deposit consisting of polymetallic vein style, manto (carbonate replacement) style, and skarn type mineralization. Host rock consists of calcareous and non-calcareous sediments of the Cassiar Platform, mainly biotite schists, limestone units, and the monzogranite unit of the Cassiar Batholith. Bulk geochemistry shows that silver concentrations are closely related to copper and antimony values, suggesting freibergite, a silver-rich endmember of tetrahedrite, is the dominant silver mineral. EPMA (microprobe) analyses identified 6 silver minerals present; silver-bearing anglesite, freibergite, diaphorite, stephanite, pyrargyrite, and silver substitution in galena. Sulfur isotope analyses of galena gave an average $\delta^{34}\text{S}$ of 6.9‰ vs VCDT, indicating a mixed mineralizing fluid source. Metal zoning patterns indicates that there is a thermal gradient across the main vein from hottest in the south-west, above the monzogranite intrusion, to coolest in the north-east. Microprobe analyses of freibergite indicates initial ore-forming fluid temperatures were between 250°C - 350°C, with subsequent cooler mineralization fluids of 170°C-200°C.

Table of Contents

ABSTRACT	1
1. INTRODUCTION	3
2. REGIONAL GEOLOGY.....	3
3. LOCAL GEOLOGY.....	6
4. METHODS.....	7
4.1. SAMPLE COLLECTION	7
4.2. SAMPLE SELECTION.....	8
4.3. SAMPLE PREPARATION	9
4.4. OPTICAL MICROSCOPE	10
4.5. WHOLE ROCK ANALYSIS	11
4.6. EPMA (MICROPROBE) ANALYSIS	11
4.7. SULFUR ISOTOPE ANALYSIS.....	12
4.8. SCANNING ELECTRON MICROSCOPE (SEM).....	12
5. RESULTS	12
5.1. GENERAL RESULTS	12
5.2. BULK GEOCHEMISTRY.....	14
5.3. EPMA (MICROPROBE)	16
5.4. SILVER BEARING MINERALS	17
5.5. SULFUR ISOTOPES.....	22
5.6. FREIBERGITE GEOTHERMOMETER	22
6. DISCUSSION.....	23
6.1. MINERAL AND METAL ZONING PATTERNS	23
6.2. LEAD ISOTOPES	25
6.3. SULFUR ISOTOPES.....	26
6.4. SILVER MINERALOGY.....	26
6.5. GEOTHERMOMETRY	28
7. CONCLUSION	30
8. REFERENCES	31
9. APPENDIX.....	33
APPENDIX A. TABLE OF SAMPLES.....	33
APPENDIX B. SAMPLE DESCRIPTIONS	34

1. Introduction

The subject of this Master's Thesis is the Silver Hart and Blue Heaven properties. Silver Hart is wholly owned by CMC Metals of Vancouver, Canada, and Blue Heaven is currently under option to CMC. The Silver Hart and Blue Heaven properties are located in the southeast of the Yukon territory of Canada. Access is provided by a gravel access road off the Alaska highway.

Prospecting in this area took off in the late 1940's as the end of World War II brought prospectors north into the Yukon following the construction of the Alaska highway. Originally the area now owned by CMC was staked for copper – tungsten skarn, but was later abandoned.

Non economical tungsten deposits are scattered throughout this region, such as the Logtung deposit to the south of Silver Hart (Mitchell et al. 2002). The CMC January 21, 2021 NI 43-101 reports total inferred resources of 7.5 million ounces (411 tons) of silver equivalent, 14.5 million pounds (6,600 tons) of lead, and 34.5 million pounds (15,650 tons) of zinc.

In total, 56 samples were collected from outcrop and drill core for this thesis. They were labeled TS-01 - TS-56 and consist of a variety of material. Samples were collected favouring galena material, but other samples from host rocks, intrusion material and massive sphalerite was also gathered.

The ultimate goal of this thesis is to study how major and minor elements are distributed throughout the property. Using the relative abundances of indicator minerals and trace elements, especially in galena, the aim is to determine if metal and mineral zoning reflects varying conditions during mineralization. This information may aid in narrowing down the most prospective areas for high-grade silver.

2. Regional Geology

The Silver Hart property is located roughly 30km north of the British Columbia border in the Yukon territory of Canada. It is situated on the northern part of the Omineca belt in what is known as the 'Rancheria District'. The Omineca belt is a Jurassic to Cretaceous age volcanic arc terrane which runs from the northern continental United States, through Canada, and into Alaska (Webster et al. 2019). The Cassiar Platform unit, in the belt, mainly consists of calcareous and epiclastic sediments from the Late Precambrian to late Paleozoic time deposited in shallow marine environment (Mortensen et al. 2007). Figure 1 below, shows a terrane map of the Yukon territory with the Silver Hart region highlighted in red.

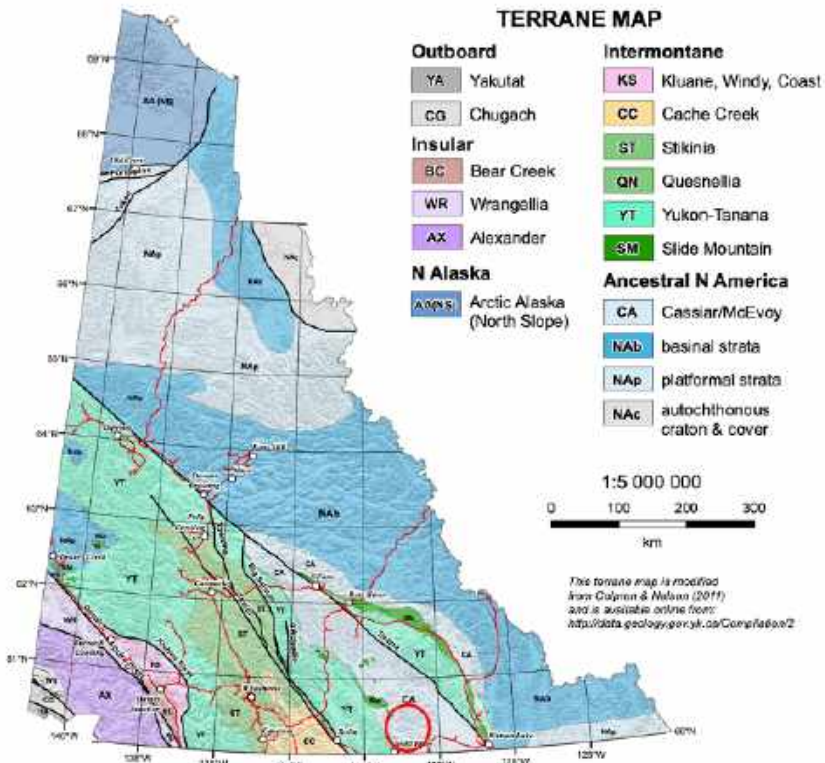


Figure 1. Terrane map of the Yukon territory showing the major Tintina fault zone (centre, diagonal), ancestral North America (upper right), and accreted terranes (lower left) (YGS 2022). Silver Hart is circled in red (bottom centre).

The Cassiar Platform (CA on map) is a piece of the North American continent that was displaced northwest by the Tintina fault (Gabrielse 1985). The platform sediments are affected by folds and thrust faults that are associated with accretion during arc-continent collision (Abbot 1983.) Larger regional scale faulting occurs in a northwest-southeast direction and is associated with the Jurassic to early Tertiary periods (Abbot 1983). Silver Hart itself lies approximately 50km southwest of the Tintina fault zone, a more than 965 km long shear zone striking roughly NW – SE with over 322 km of displacement (Roddick 1967). The Tintina fault separates the Cassiar Platform from the Selwyn Basin (NAb in map). The Cassiar Batholith is a large intrusive plutonic body of approximately 100 Ma. (Driver et al. 2000). It is mainly composed of coarse-grained quartz monzonite, with pink orthoclase megacrysts, and coarse-grained biotite-hornblende granodiorite (Nelson 1986). Figure 2 below, details mining and exploration activity in the Yukon territory.

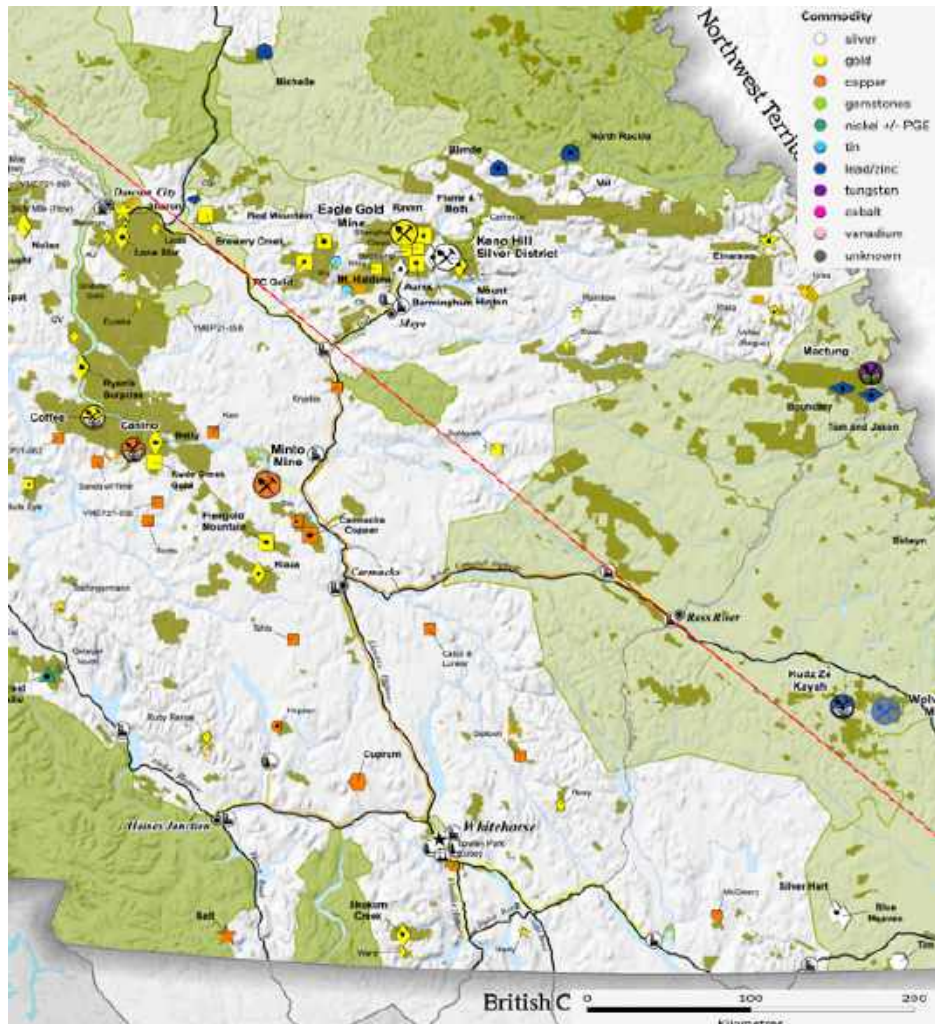


Figure 2. Current mining and exploration activity in the Yukon Territory of Canada. Past producers, such as the Faro mine are not shown. Silver deposits are shown in white, lead/zinc in blue, Gold in yellow, and copper in orange (YGS 2022). Red line shows the approximate location of the Tintina Fault.

3. Local Geology

Figure 3 below, shows a 50km by 50km bedrock geology map of the Silver Hart property, and the surrounding area.

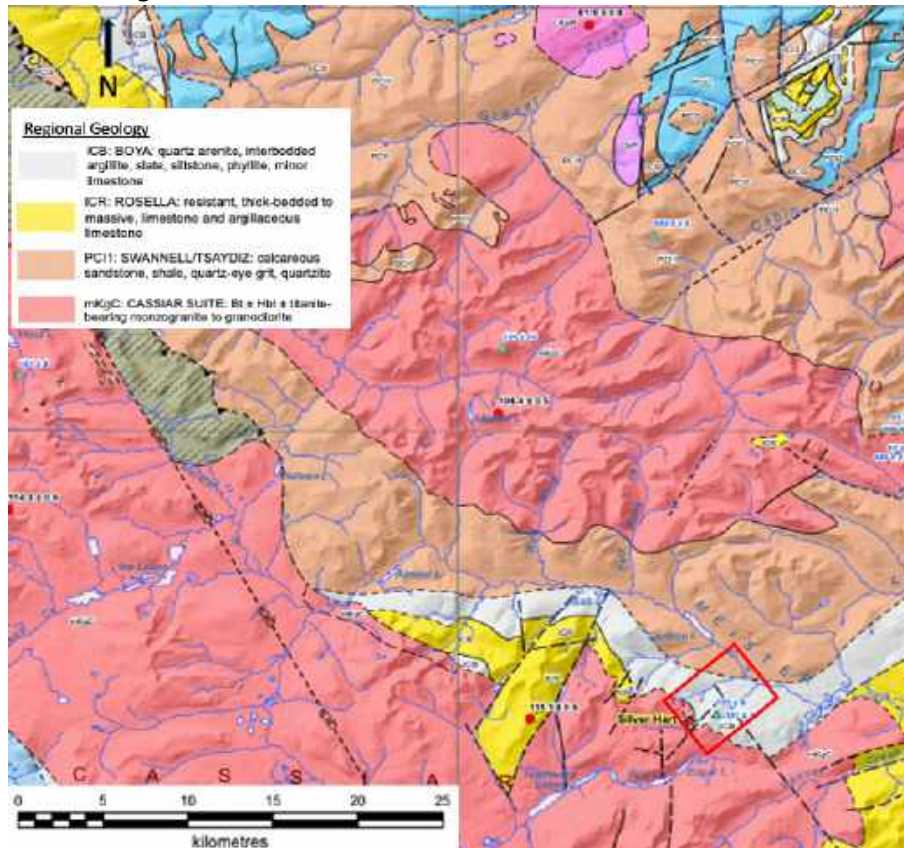


Figure 3. Bedrock geology map of the Silver Hart property (lower right) and surrounding area (YGS 2022).

Silver Hart lies on the boundary between the Cassiar Platform and Cassiar Batholith. The South and West parts of the property comprise mainly granodiorite from the Cassiar Batholith. To the East and North, rocks are calcareous and epiclastic metasediments of the Cassiar Platform; quartz arenite, interbedded argillite, slate, siltstone, phyllite, limestone, and rarely conglomerate (YGS 2022). Limestone is common at Silver Hart as a 200 to 500 meter wide layer of Cassiar Platform sediments. Carbonate replacement galena can be found in multiple locations throughout this limestone.

Alternating bands of carbonate and schist units strike northwest – southeast, roughly parallel to the strike of larger regional faulting such as the Tintina trench. Due to the high altitude and mountainous terrain of the area, bedrock may be exposed at surface, especially at higher elevations where the terrain is treeless.

Numerous silver-lead-zinc deposits are found along the strike of the Cassiar Platform boundary from northern British Columbia, and further north-west to the historic world class deposits of Keno City. In general these deposits are calcareous and non-calcareous sediment hosted deposits with galena, and silver minerals such as freibergite and pyrargyrite. Freibergite was the major silver ore mineral in the Keno City district (Lynch 1989).



Figure 4. Zones of mineralization at Silver Hart.

4. Methods

4.1. Sample Collection

During the summer of 2021, 56 samples for this thesis were collected. All samples were collected by Michael Ives-Ruyter. The samples were collected directly from bedrock in keeping with best practices to avoid collecting transported material. All samples were photographed upon collection. Photos are included in appendix A2 and show the sample, sample number, and the immediate terrain around the sample.

Each Sample was then placed in a heavy-duty polypropylene ore bag marked with an ID number in permanent marker. An additional unique identifying tag was added to each bag, and they were then secured with a zip-tie. GPS location was recorded with a Garmin GPSMAP 65 and in a rite-in-the-rain waterproof notebook along with a brief description on the sample and area. Photos were also taken of the notebook to ensure that important information was recorded in multiple locations, adding an extra layer of redundancy. A GIS map was also made, showing the location of each sample against a high-definition photo of the terrain. Figure 5 below, shows where samples were collected on the Silver Hart and Blue heaven properties.

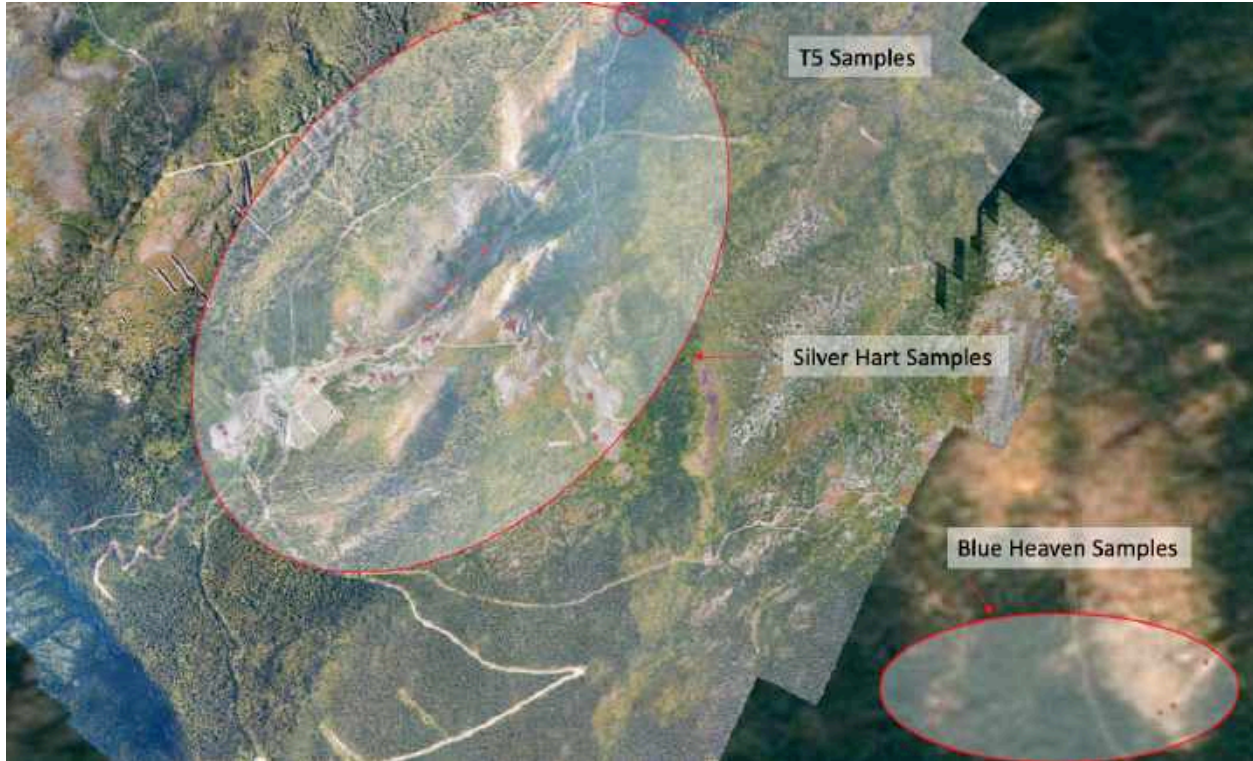


Figure 5. Sampling locations on Silver Hart and Blue Heaven.

Batches of 10 samples were placed in large rice bags, secured with a zip-tie, and wrapped with fluorescent flagging tape. Mr. Wade Carrell, of CMC Metals transported these samples to Whitehorse Yukon, packed each rice bag into a 5 gallon pail, secured each pail with a sturdy lid, and sent them through Canada Post to Luleå Tekniska Universitet (LTU) in Luleå, Sweden.

TS-01 through TS-45 were collected from various areas of Silver Hart. They consisted of representative samples from every major mineral occurrence on the property, many occurrences of minor mineralization of galena and sphalerite, plus several samples of non-mineralized rock. The non-mineralized samples consist of granodiorite, skarn, schist, quartz breccia, carbonate breccia, and limestone.

Samples TS-45 to TS-50 are all cut from a single drill core on T5.

Samples TS-51 to TS-56 were collected from the Silver Hart sister property, Blue Heaven. These samples consist of disseminated to massive galena, disseminated to massive sphalerite, manganese-stained material, and host rock. Samples from Silver Hart and Blue Heaven will be compared to study their similarities and differences.

4.2. Sample Selection

Upon arrival at LTU, each sample was carefully unpacked and checked. No samples or polypropylene bags were damaged during shipping. Every sample was then cut with a diamond saw and inspected on their cut face. Sample ID's were written on each piece of rock that was cut. Of these 56 samples collected, 34 were selected to make into polished pucks, and 18 were selected for elemental analysis. A circle was drawn around the target area with a permanent marker to ensure that the area of interest was properly cut from the larger sample rock. The majority of the polished pucks (29) show mineralization of some kind (galena, sphalerite, pyrite, or manganese).

4.3. Sample Preparation

Each sample was cut down firstly with a large diamond circular saw, and then with a smaller diamond circular saw to a hockey puck shape with a diameter of 1.5 to 2cm. Each puck was marked with the sample ID immediately after cutting, and placed in a small plastic bag also marked with sample ID. Hot epoxy mounting methods usually use temperatures in excess of 200°C and pressures in excess of 250 bar to mount samples. Because of this, hot epoxy was avoided as it may change textures, structures, or alter geothermometry data that will be used to help determine formation temperature of these minerals. Each sample was placed in a two-piece, 25mm Struers cold epoxy mounting cup. Sample ID's were written on each mounting cup to ensure sample accuracy. Under a fume hood, Struers Epofix resin was mixed with Epofix hardener at a ratio of 25:3 (resin to hardener). This mixture was stirred in a paper cup with a wooden stir-stick for 2 minutes. Each of the puck molds was then filled with the epoxy mixture. The filled cups were placed into a Struers CitoVac vacuum impregnation unit. The machine was cycled between 0.14 bar vacuum and approximately 1 bar (atmospheric pressure) 20 times and then held at 0.14 bar vacuum for 5 minutes. This was done to force epoxy into the porous spaces of the samples. The samples were then left for a minimum of 24 hours to assure proper curing of the epoxy. Using gentle heat from a Struers Drybox 2, the sample preparation cups were separated and the samples were extracted from the cups. A firm strike from a hammer was necessary in most cases to extract the samples from the molds. Immediately after extraction, the sample ID was permanently written on each puck with a tungsten tipped scribe. Samples were extracted and inscribed one by one to avoid the possibility of mislabeling. A Struers Discoplan-TS cutting and grinding saw was used to cut the puck thickness down to approximately 15mm.

A Struers LaboForce 100 automatic grinding and polishing machine was used for the final steps in producing polished pucks. The first step was rough grinding, which involved grinding 6 samples at a time using a Struers MD-Piano 200 grit grinding disk with water. A force of 10N and a rotation speed of 75 RPM was used in both the rotating head and the rotating disk. Opposite rotation direction in the head and disk was used. As this was a very aggressive abrasive, grinding was done 3 minutes at a time. Then samples were checked under a Leica stereoscopic microscope to ensure epoxy was removed from the face of the sample. Struers MD-Piano 550 grit and 1200 grit were then used sequentially to further reduce scratches on the sample face. Grinding settings for 550 and 1200 grit were the same as for 200 grit, but a longer grinding period was used, usually between 7 and 14 minutes before checking the samples under a stereoscopic microscope.

The same LaboForce machine was used for sample polishing. MD-Pan polishing pads were used with Struers diamond polishing media. Polishing began with a 9µm polishing pad and media. The pressure was increased to 15N and polishing time was increased to 15 minutes. After each round of polishing, the samples were inspected under a microscope to ensure large scratches were polished out. The same steps were repeated with a 3µm polishing pad and media and finally a 1µm polishing pad and media to completely remove scratches and provide a mirror finish. Figure 6 below, shows a typical completed polished puck of galena in epoxy.

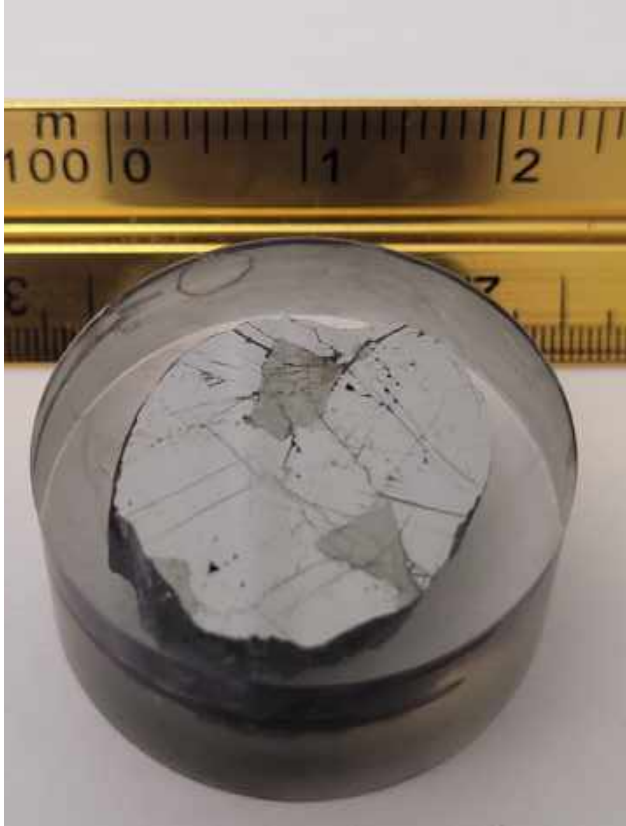


Figure 6. A typical completed polished puck (TS-03, Galena with large freibergite grains).

4.4. Optical Microscope

Prepared pucks were initially examined under a Leica transmitted/reflected light microscope with an attached camera. This was done for two reasons. Firstly, because a much lower magnification can be used with an optical microscope (10x) compared to an SEM (~100x), samples can be scanned much more quickly to determine areas of interest for later study and analysis. Secondly, and more importantly, an optical microscope can show colour, while an SEM cannot. This allowed for the quick detection of chalcopyrite, pyrite, and deformation in calcite grains which indicated an upper temperature limit. Figure 7 below, is polished puck TS-29 under optical microscope with reflected light, showing blebby freibergite in galena, sphalerite and chalcopyrite.

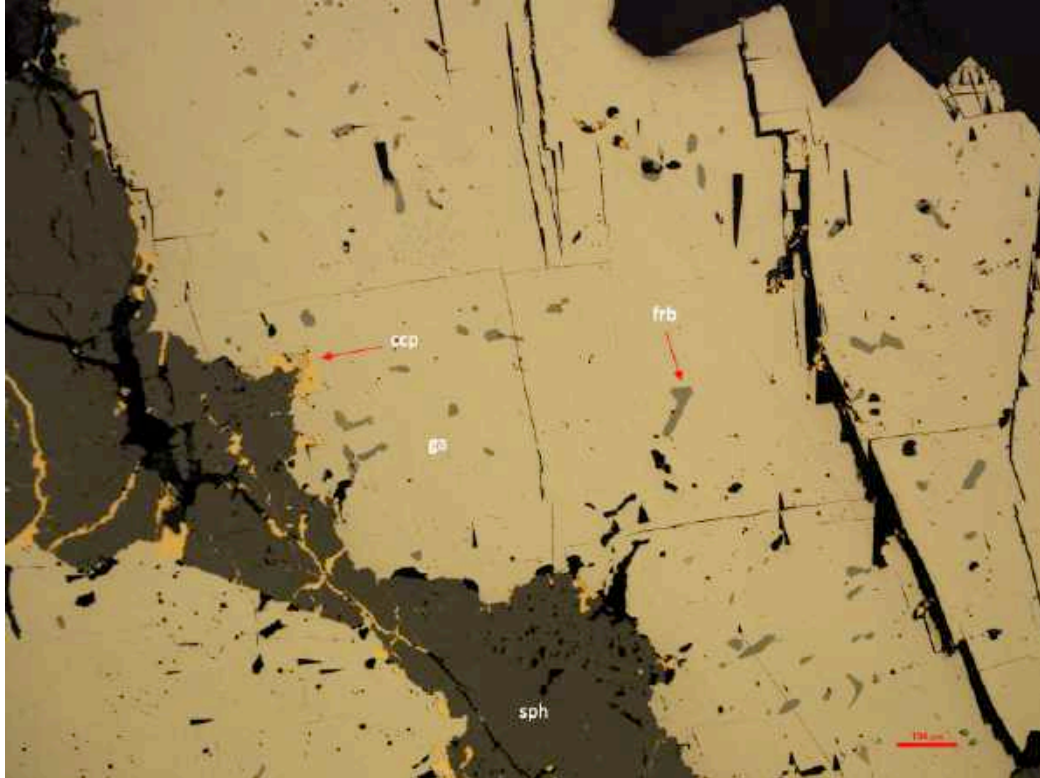


Figure 7. Reflected light photo (sample TS-29) of freibergite (frb) inclusions in galena (ga), sphalerite (sph), and chalcocopyrite (ccp). Scale bar is 100 microns.

4.5. Whole Rock Analysis

To determine total elemental abundances, 18 samples were sent to ALS for bulk geochemistry. Care was given to ensure that as little dilution as possible occurred from the presence of gangue minerals, therefore making comparisons between samples as accurate as possible. In certain cases like TS-52, which has disseminated galena, this wasn't possible. But the most galena rich portion of the sample was sent for assay.

Samples were cut into roughly equal size portions, placed in polypropylene bags and sealed with zip ties. Each sample was marked with a sample number both on the rock itself in permanent marker, and on the sample bag. A portion of each sample was kept in order for results to be replicated.

The assay methods chosen were ME-MS61 four acid digestion followed by ICP-MS analysis for samples that had mixed compositions, and ME-ICPORE four acid digestion followed by ICP-MS analysis for massive galena samples, which can better tolerate high sulfide concentrations. Over-limit (ore grade) OG62 analyses were conducted for silver, lead, copper, and zinc. Additionally, ME-CON02 (for very high concentrations) assays were conducted for silver and lead, as those concentrations were up to 1% and 84.2% respectively (ALSglobal.com).

4.6. EPMA (Microprobe) Analysis

For spot chemical analysis of selected minerals, 10 polished pucks were sent to the Geological Survey of Finland (GTK) for microprobe analysis. Each sample was individually wrapped in soft tissue paper and carefully packaged in a box to avoid scratching the puck surface. High resolution photograph scans of the samples were included. These scans showed exactly which locations were to be analysed. At GTK, the samples were carbon coated to ensure electron dispersion on the sample face.

Samples were analysed with a Cameca SX100 electron microprobe analyser (EPMA) using wavelength dispersive spectroscopy (WDS). Accelerating voltage and beam current were 20 kV and 40 nA respectively and a beam diameter of 5 microns for sulfide minerals. Accelerating voltage and beam current were 20 kV and 10 nA respectively for minerals with high silver content, and a beam diameter of 2 or 10 microns depending on grain size (GTK 2022).

In total 92 measurements were made, generally favouring sphalerite and galena. The aim of the microprobe analysis was to apply the GGIMF (gallium, germanium, indium, manganese, iron) geothermometer, and the cadmium ratios of sphalerite and galena to determine the temperature of crystallization at Silver Hart in various mineralized zones.

4.7. Sulfur Isotope Analysis

To determine mineralizing fluid source, 6 samples of massive galena were selected for $\delta^{34}\text{S}$ isotope analysis. Each of the samples was first cut down to a cube of galena with a rock saw to ensure outside contamination was removed. The sample was then struck with a hammer in order to fracture the galena grains along natural cleavage faces, ensuring the sample was a monomineralic as possible. Several grains from each sample were hand-picked and placed in small polyethylene sample bags with the sample number written on the bag in permanent marker. The hammer and all surfaces were cleaned thoroughly between each sample to ensure that galena from one sample didn't contaminate any other.

The samples were then sent to the Queen's Facility for Isotope Research at Queen's University in Kingston, Canada for analysis. The sulfur isotopic composition were determined using a MAT 253 Stable Isotope Ratio Mass Spectrometer with a Costech ECS 4010 Elemental Analyzer. The $\delta^{34}\text{S}$ composition was then determined by normalizing $^{34}\text{S}/^{32}\text{S}$ sulfur ratios to that of a known standard, in this case the Vienna Canyon Diablo Troilite (VCDT), a well-known international standard. Blanks and standards were used to ensure accuracy, and results are replicable to 0.2‰ (Queen's University 2022).

4.8. Scanning Electron Microscope (SEM)

Samples were examined with a Zeiss Sigma 300VP scanning electron microscope, equipped with a Bruker XFlash 6160 analyser. A total of 9 samples were loaded onto a mounting cassette at once and placed in the SEM. A reference photo of the samples was uploaded to the computer and used to navigate between and within samples. Backscatter Electron Detector (BSD) mode was used with a working distance of 8.5 mm, and an accelerating voltage (EHT) of 20 kV. High resolution photos were taken with Zeiss software and were named according to sample number and what was being observed. Bruker analyses were made and photographed using separate Bruker software. All mineralized samples were studied with the SEM which also helped to determine which samples were to be sent for microprobe analyses.

5. Results

5.1. General Results

Optical microscopy suggests that the majority of silver occurs as small inclusions of silver-bearing sulfosalts within galena. These inclusions generally range in size from $\sim 100\ \mu\text{m}$, down to less than $1\ \mu\text{m}$. Samples TS-02 and TS-03 were the only samples that had large sulfosalts grains greater than 2 mm. In some cases like figure 8 (below) these inclusions appear to follow a trend.

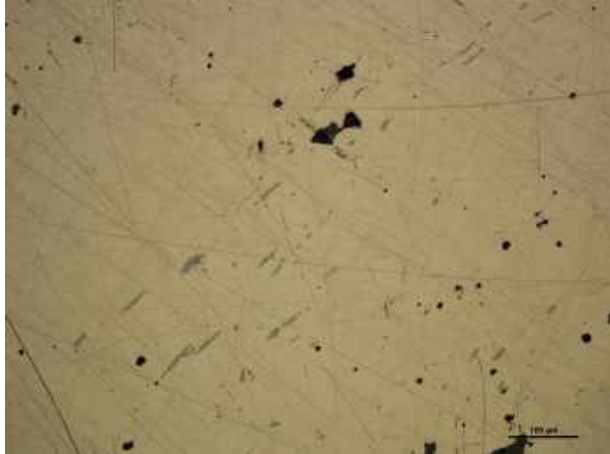


Figure 8, aligned sulfosalt inclusions in galena, sample TS-17.

In general, silver is strongly associated with galena. Every sample with disseminated to massive galena that was analyzed by SEM, microprobe, or bulk geochemistry showed elevated silver concentrations. The elevated silver abundances were accompanied by similar elevations in copper and antimony, suggesting that freibergite is prevalent in galena throughout the Silver Hart property. Galena is also commonly associated with sphalerite and chalcopyrite. In general, copper is more abundant in sphalerite where it is in contact with galena. Boundaries between galena and sphalerite occur both as simple and sharp contacts, shown in figure 9a, and as irregular contacts in figure 9b.

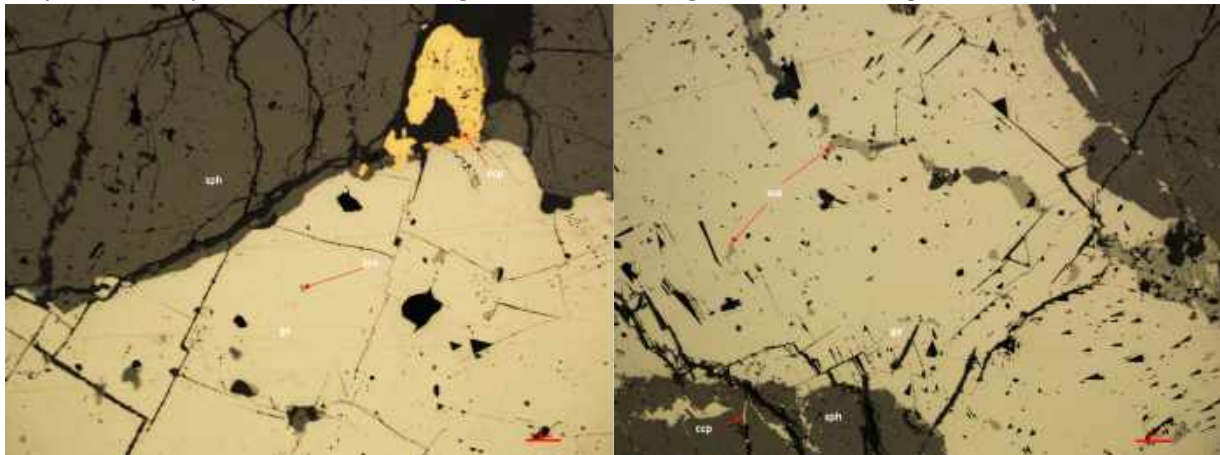


Figure 9a (left), showing sharp contact between galena (ga) and sphalerite (sph), and figure 9b (right), with irregular contact relation between galena and sphalerite. Also shown is chalcopyrite (ccp), and unknown sulfosalts (ssa), likely freibergite in samples TS-02 (left) and TS-01 (right).

Evidence of ductile deformation is also visible in the polished pucks of several samples. In figure 9a (above left) the normal cubic cleavage of galena is plastically deformed into wavy cleavage plains. Tracing these fractures up into sphalerite shows that sphalerite underwent brittle fracturing, likely from the same deformation event.

5.2. Bulk Geochemistry

The analytical results of the bulk geochemical assays are summarized in Table 1, below.

Table 1. Bulk geochemical assay results for a selection of elements (red equals a higher concentration).

SAMPLE	Ag ppm	Cu ppm	Fe %	Mg %	Mn ppm	Pb %	S %	Sb ppm	Zn %	As %	Hg ppm	Zone
TS-01 (sph and galena)	1920	3500	10.75	0.05	22300	0.137	15.75	630	29.8	0.395	<8	Old Shaft
TS-02 (sph and galena)	11050	17750	2.14	0.04	3460	19.15	20	15250	31.4	0.323	8	Old Shaft
TS-03 (massive galena)	7950	6560	0.66	0.04	1580	82.5	12.95	10450	0.365	0.021	<8	TM
TS-08 (galena vein)	4910	3980	0.5	0.05	<50	53	14.3	6040	6.5	0.165	14	TM
TS-11 (quartzite with chalcopyrite)	177	2030	1.17	0.03	41	1.57	1.76	238	2.1	0.923	0.065	H
TS-14 (massive galena)	7780	5140	0.18	0.04	<50	76.2	13.25	9670	1.345	0.015	<8	S
TS-16 (massive galena)	1180	1480	0.81	0.05	<50	82.6	13.7	1160	0.744	<0.005	11	S
TS-17 (massive galena)	3030	150	0.48	0.04	340	84.2	13.1	3130	0.094	<0.005	9	M
TS-23 (massive galena)	1835	610	0.09	0.05	50	76.6	8.65	1150	0.091	<0.005	<8	JD
TS-29 (galena vein in matrix)	704	476	6.31	0.36	20500	18.25	5.58	558	4.44	0.0745	0.039	WWM
TS-30 (pyrite in schist)	40.59	326	24.5	1.1	417	0.101	>10.0	4.02	0.0094	0.00021	0.009	TM/K
TS-35 (massive galena egg)	1380	2030	1.24	0.01	1320	78.2	13.25	4830	1.6	0.025	<8	TM/K
TS-38 (host rock, quartz breccia)	50.6	539	2.81	0.13	974	0.1845	7.73	82	14.05	>1	0.218	TM/K
TS-42 (massive galena)	6890	2690	1.08	0.04	23000	71.8	9.01	2500	0.123	0.018	<8	K
TS-44 (massive galena)	3270	2510	1.74	0.06	580	29.4	7.55	2360	0.034	0.005	<8	KL
TS-45 (granodiorite intrusion)	1580	1185	1.91	0.13	600	>20	3.51	>250	0.0165	0.00223	0.028	TS
TS-51 (massive galena BH)	994	290	0.64	<0.01	120	70.8	11.8	1060	0.688	0.008	<8	Blue Heaven
TS-52 (disseminated galena BH)	7270	11100	2.15	0.01	44	16.25	4.69	>10000	0.267	>1	0.043	Blue Heaven

The results for selected elements are shown in Figure 10 below, with samples distributed along the vein system from SW to NE.

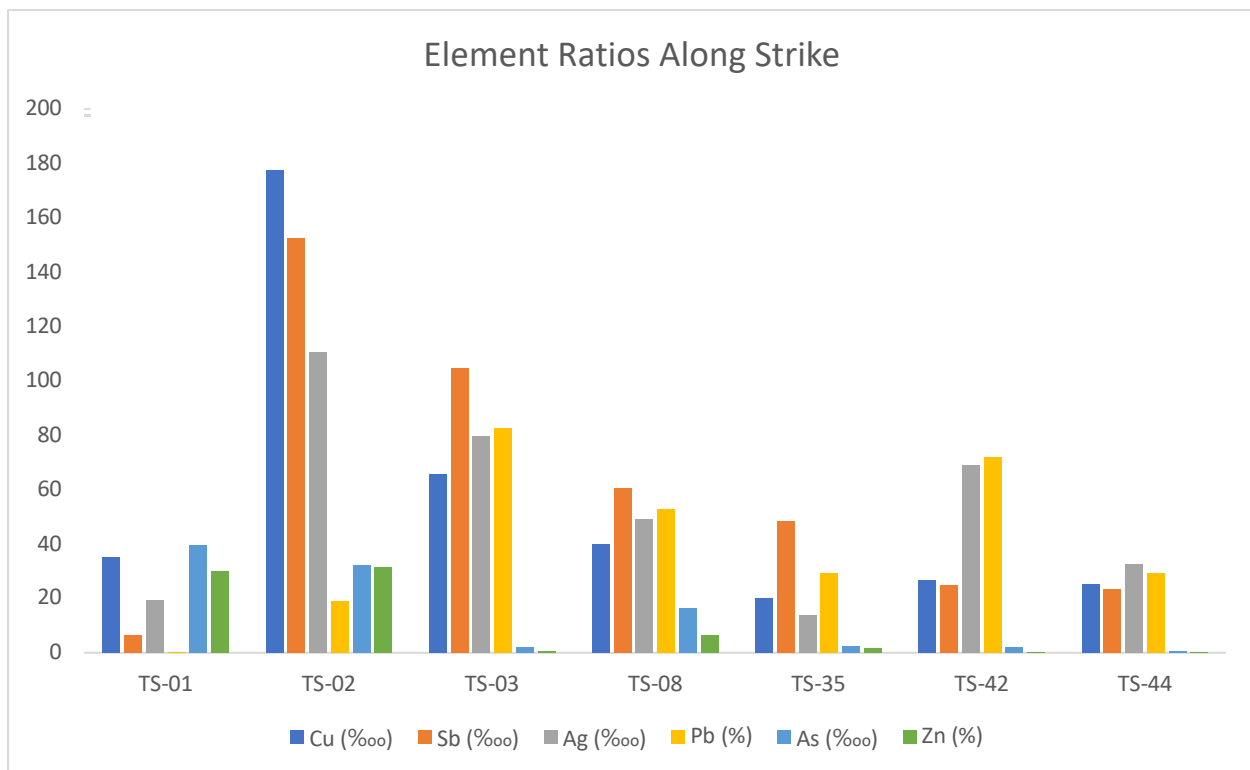


Figure 10. Content of selected elements along the vein system (SW to NE) based on bulk assays. Lead and zinc concentration in percent, others in permyriad, parts per 10 thousand (‰).



Figure 11. Locations along the TM-K-KL main vein system where galena samples were collected for figure 10 (above).

Geochemical analysis of the Cassiar Batholith intrusion was used to calculate the normative mineral composition, which was found to be; 32.7% quartz, 26.50% plagioclase feldspar, and 37.30% alkali feldspar.

While this intrusion is commonly classified as granodiorite, on a Q-A-P ternary plot, sample TS-45 plots in the monzogranite field. Figures 12a&b, below show a Q-A-P diagram with sample TS-45.

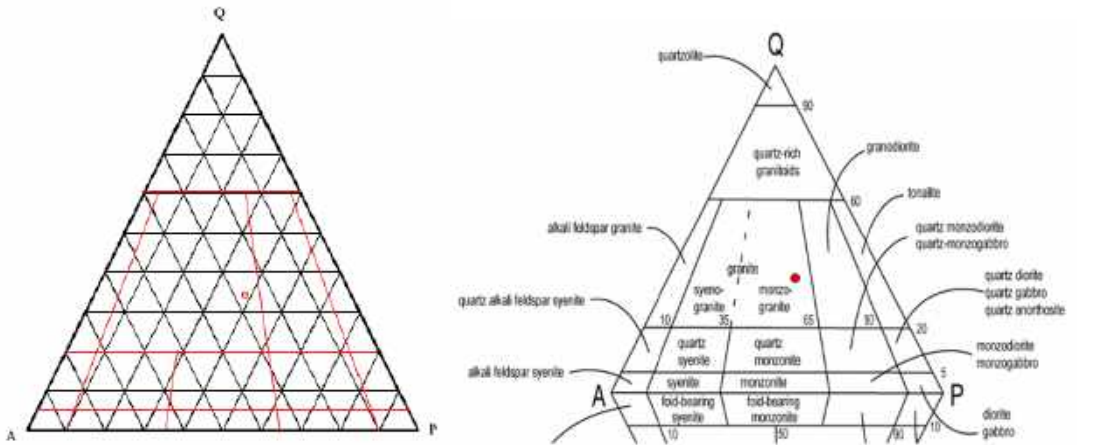


Figure 12a (left), Q-A-P diagram as calculated in Excel, and figure 12b (right) showing where TS-45 plots on a Streckeisen diagram (Le Bas and Streckeisen 1991).



Figure 13. Typical monzogranite rock of the Cassiar Batholith in core (CMC21-T5 212.45-212.8m).

5.3. EPMA (Microprobe)

Substitution of silver for lead in galena does occur at Silver Hart, but was found to generally be less than 0.25 atomic %.

Antimony is also present in galena in concentrations up to about 0.4%, suggesting that coupled substitution of Ag^+ and Sb^{3+} for $2Pb^{2+}$ (Sharp and Buseck 1993). Figure 14, below, shows Ag-Sb ratios in various galena samples at Silver Hart with a general trend of decreased concentrations towards the northeast. The microprobe analyses suggest that a significant part of the silver content in the veins occurs as silver-bearing sulfosalts. These inclusions are generally 10-30% silver by atomic percentage, and exist in every galena sample analysed.

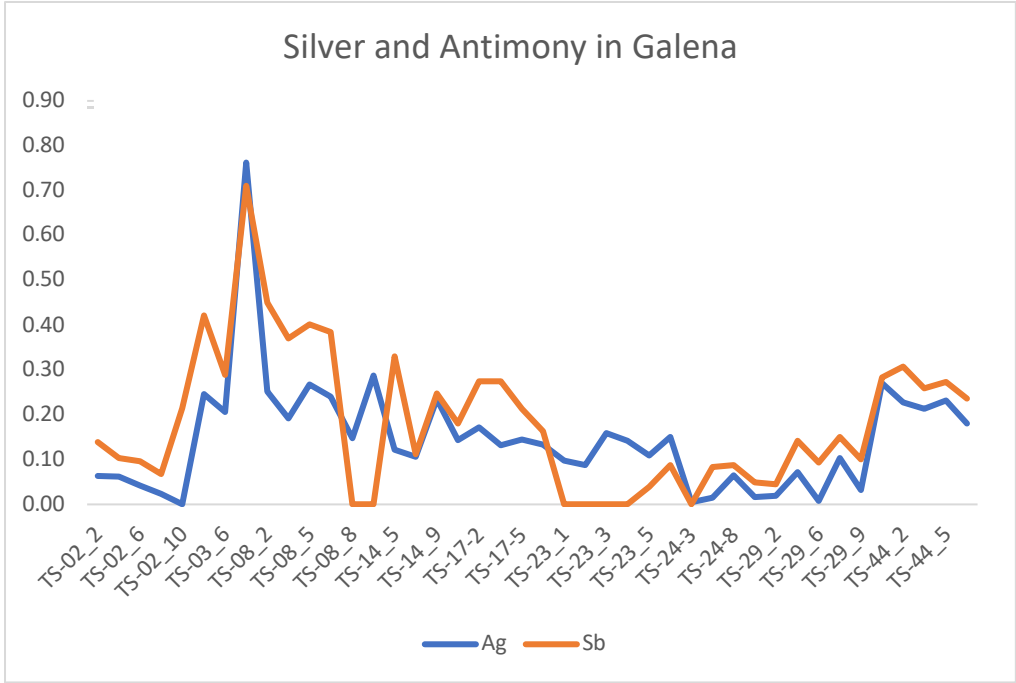


Figure 14. Variation in silver and antimony in galena as a result of substitution along the vein system from SW to NE.

5.4. Silver Bearing Minerals

Electron microprobe and SEM results suggest that silver occurs in at least 6 different silver-bearing minerals, they are:

1) Silver bearing anglesite (PbSO_4) occurring between grains of galena. This mineral is common between oxidised grains of galena and in some cases can form long continuous veins. EDS analyses show that where anglesite is plentiful, the amount of silver contained within it is very low. When anglesite occurs as small inclusions, such as in figure 15 a-d below, silver concentrations may be much higher. This is likely a dilution effect as lead, sulfur, and oxygen are far more plentiful in the system compared to silver.

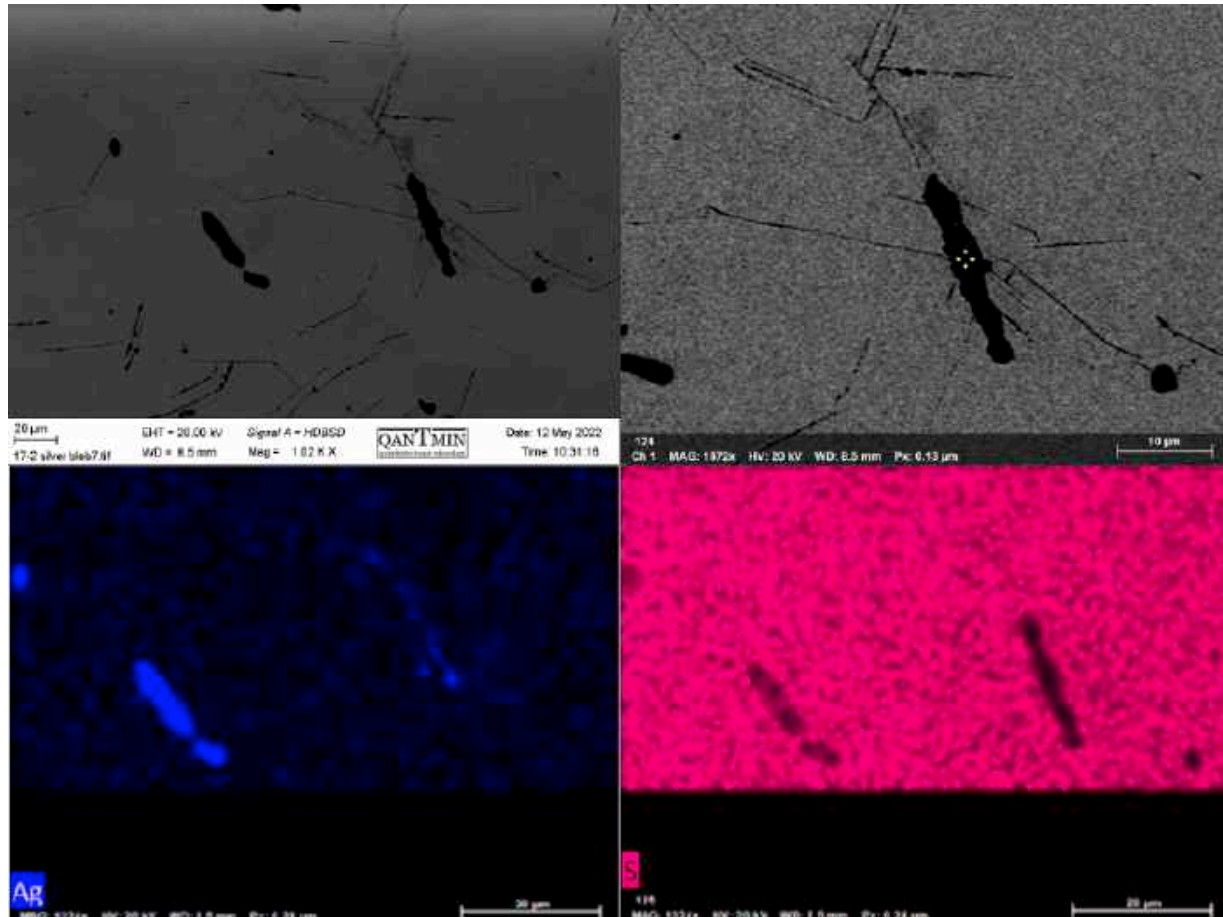


Figure 15a top left, high resolution photo of a silver bearing anglesite inclusion in galena (centre-right of frame). From sample TS-17, taken from M zone. Figure 15b top right, location of analyses shown in table 2 below. Figures 15 c&d, bottom left and bottom right, showing slight silver enrichment, and lead dilution relative to surrounding galena.

Table 2. Composition of silver bearing anglesite.

Element	At. No.	Netto	Mass [%]	Mass Norm. [%]	Atom [%]	abs. error [%] (1 sigma)	rel. error [%] (1 sigma)
Carbon	6	4036	0.00	0.00	0.00	0.00	10.00
Oxygen	8	2241	6.17	7.13	34.43	1.16	18.86
Sulfur	16	19850	9.12	10.55	25.39	0.36	3.97
Molybdenum	42	0	0.00	0.00	0.00	0.00	1.54
Silver	47	17029	17.34	20.05	14.35	0.59	3.39
Antimony	51	7091	8.69	10.05	6.38	0.30	3.50
Lead	82	7449	45.14	52.21	19.45	1.51	3.34
		Sum	86.45	100.00	100.00		

2) Pyrargyrite (Ag_3SbS_3) containing up to 60wt% silver. This mineral is found in blebby inclusions in galena. Figure 16a below, shows a typical pyrargyrite inclusion. This inclusion appears isolated within the surrounding galena crystal distant from veins and cracks, suggesting that pyrargyrite exsolved from the surrounding galena. Microprobe analyses of galena in this sample shows up to 0.16wt% silver and 0.28wt% antimony, further supporting the exsolution hypothesis.

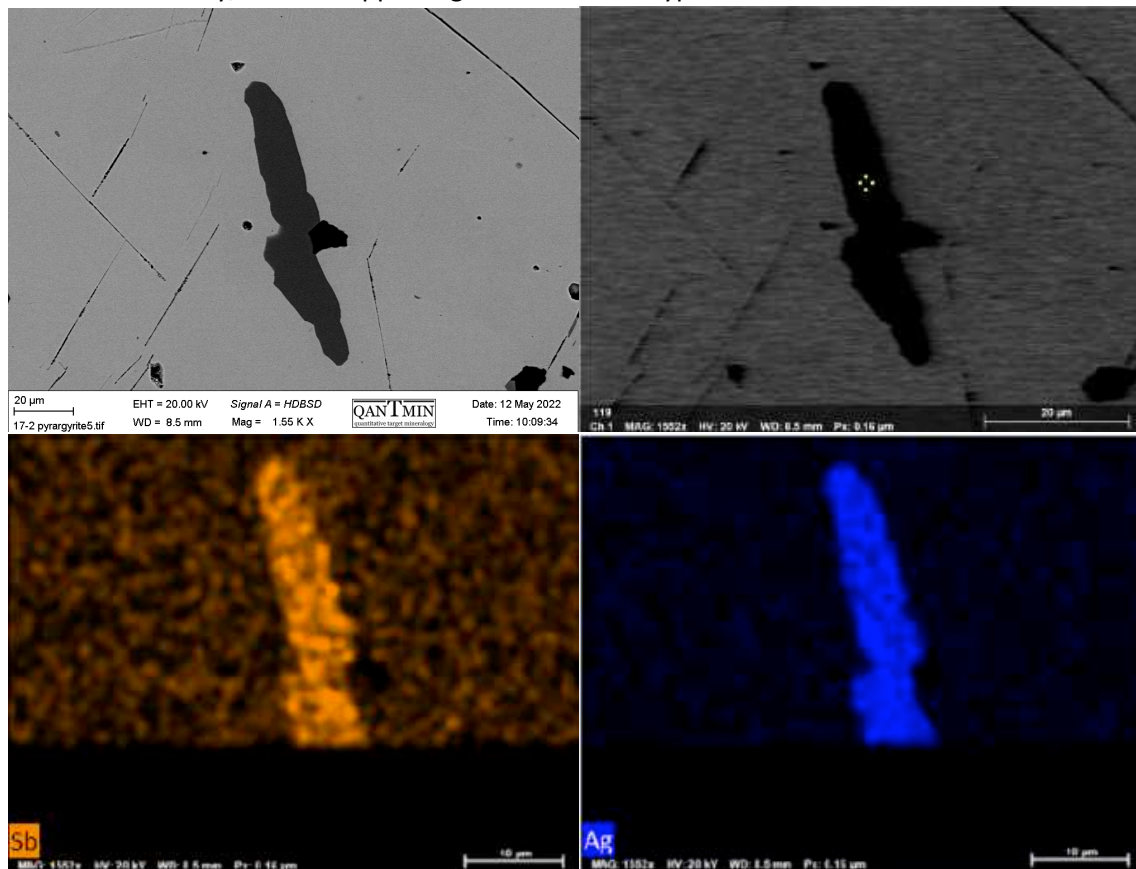


Figure 16a top left, high resolution photo of a pyrargyrite inclusion in galena. From sample TS-17, taken from M zone. Figure 16b top right, location of analyses shown in table 3 below. Figures 16c&d, bottom left and bottom right, showing where the highest concentrations of silver and antimony occur.

Table 3. Composition of pyrrargyrite inclusion.

Element	At. No.	Netto	Mass [%]	Mass Norm. [%]	Atom [%]	abs. error [%] (1 sigma)	rel. error [%] (1 sigma)
Carbon	6	1779	0.00	0.00	0.00	0.00	10.00
Aluminium	13	1969	1.32	1.43	4.39	0.10	7.68
Sulfur	16	31554	13.95	15.20	39.16	0.53	3.83
Arsenic	33	321	1.21	1.31	1.45	0.11	8.84
Silver	47	53519	44.07	48.01	36.77	1.41	3.21
Antimony	51	13337	15.31	16.68	11.32	0.50	3.23
Lead	82	2330	15.93	17.36	6.92	0.64	4.01
		Sum	91.78	100.00	100.00		

3)Freibergite $(Ag, Cu, Fe)_{12}(Sb, As)_4S_{13}$ is part of a large series of sulfosalts with high elemental variability. This mineral appears frequently in galena samples. It is common as blebs scattered throughout galena, down to only a few microns in size. Figures 17 a-c below show several blebs of freibergite in sample TS-29, galena from the WWM zone.

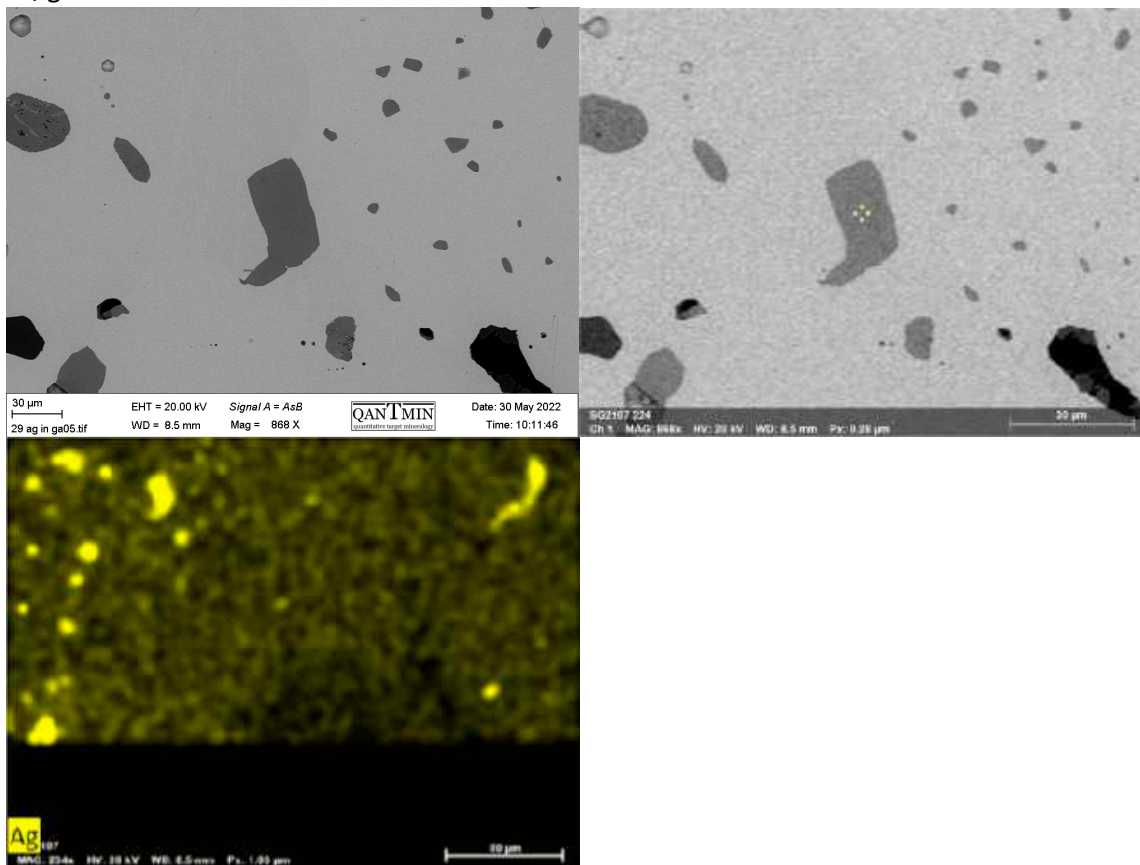


Figure 17a top left, high resolution photo of a freibergite inclusion in galena. From sample TS-29, taken from WWM zone. Figure 17b top right, location of analyses shown in table 4 below. Figure 17c, bottom left, showing where the highest concentrations of silver occur.

Table 4. Composition of freibergite inclusion.

Element	At. No.	Netto	Mass [%]	Mass Norm. [%]	Atom [%]	abs. error [%] (1 sigma)	rel. error [%] (1 sigma)
Carbon	6	936	0.00	0.00	0.00	0.00	10.00
Oxygen	8	857	2.45	2.82	12.64	0.61	24.68
Sulfur	16	35303	14.87	17.11	38.24	0.57	3.81
Iron	26	2005	2.24	2.57	3.30	0.11	4.76
Copper	29	1932	3.27	3.77	4.25	0.15	4.46
Zinc	30	847	1.62	1.86	2.04	0.10	6.22
Arsenic	33	415	1.56	1.79	1.72	0.12	7.75
Silver	47	32501	26.70	30.72	20.41	0.87	3.28
Antimony	51	12827	13.61	15.66	9.21	0.44	3.26
Lead	82	2993	20.60	23.70	8.20	0.78	3.81
		Sum	86.92	100.00	100.00		

Freibergite can also occur as large well-defined crystals, several millimeters in size. Figures 18 a-d below, show an SEM photo and spectral analysis of a large freibergite crystal surrounded by galena.

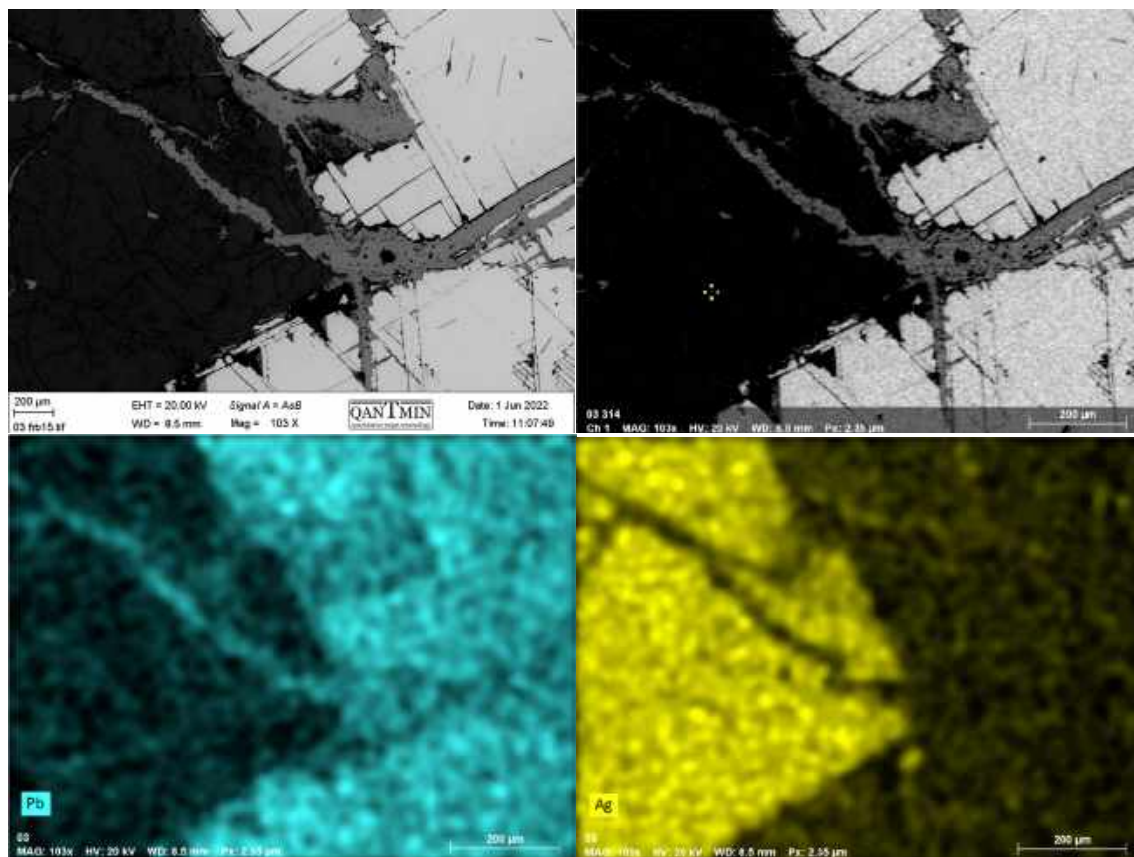


Figure 18a top left, high resolution photo of freibergite (black mineral) and galena. Light grey vein is likely anglesite (PbSO_4). Sample TS-03, taken from TM zone. Figure 18b top right, location of analyses shown in table 5 below. Figures 18c&d, bottom left and bottom right, showing lead-rich area (galena) and silver-rich area (freibergite).

Table 5. Composition of large euhedral freibergite grain in TS-03.

Element	At. No.	Netto	Mass [%]	Mass Norm. [%]	Atom [%]	abs. error [%] (1 sigma)	rel. error [%] (1 sigma)
Carbon	6	1673	0.00	0.00	0.00	0.00	10.00
Magnesium	12	297	0.26	0.37	0.94	0.05	19.10
Sulfur	16	49034	14.35	20.03	38.77	0.54	3.80
Iron	26	3415	3.51	4.90	5.45	0.14	3.99
Copper	29	13062	22.15	30.90	30.18	0.66	2.96
Zinc	30	1167	2.20	3.08	2.92	0.12	5.37
Silver	47	20723	10.74	14.99	8.62	0.37	3.46
Antimony	51	27241	18.45	25.74	13.12	0.57	3.12
		Sum	71.66	100.00	100.00		

4) Stephanite (Ag_5SbS_4). Unfortunately, an EDS analysis was not done with the SEM. However, a photo was taken, and the mineral was later analysed by microprobe in Finland. It was found to contain 69.62% silver, 9.06% antimony, and 14.14% sulfur by weight. Stephanite contains 68.33% silver, 15.42% antimony, and 16.25% sulfur by weight (webmineral.com). Stephanite occurrences were noted in the silver mines of Keno City, 450km north-west of Silver Hart (Lynch 1989). Figures 19a&b below, show a small inclusion of stephanite in galena from sample TS-03. The only other occurrence of stephanite is in TS-09, a sample of wall rock.

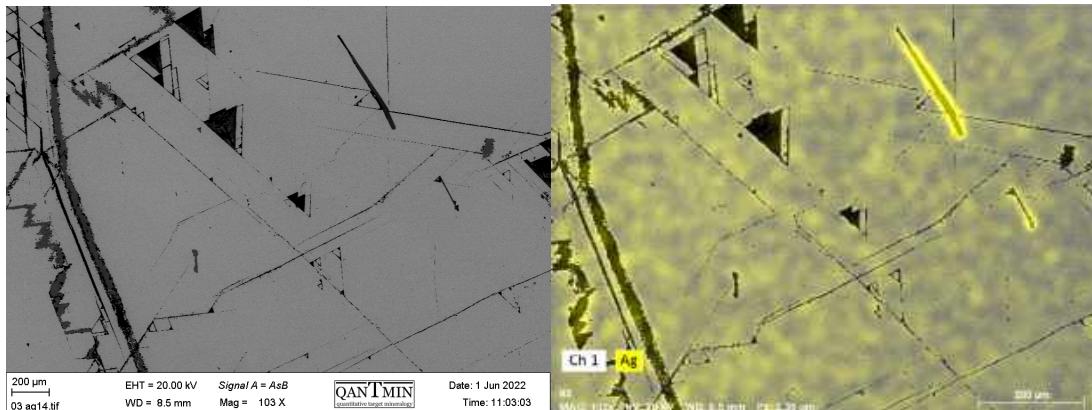


Figure 19a left, stephanite in galena (elongated inclusions in top left) and figure 19b right, highlighting stephanite.

5) Diaphorite ($\text{Ag}_3\text{Pb}_2\text{Sb}_3\text{S}_8$). This mineral was not identified with the SEM due to the very small size of the mineral. It was found by microprobe and is covered further in section 6.5.

6) Silver substitution of lead in galena crystal lattice. Table 6 below, shows the average concentration of silver in galena samples. The data was collected by microprobe analysis and targeted clean areas of galena, absent of cracks and inclusions.

Table 6. Silver in galena due to substitution of Pb^{2+} by Ag^+ .

sample	Ag av in ga
TS-02	0.04
TS-03	0.37
TS-08	0.21
TS-09	no galena
TS-14	0.14
TS-17	0.13
TS-23	0.11
TS-24	0.02
TS-29	0.04
TS-44	0.21

The average silver concentration in galena due only to substitution is 0.15wt%, but varies from 0.37 to 0.02wt% with a generally decreasing trend from SW to NE.

5.5. Sulfur Isotopes

To determine the source of mineralizing fluids, 6 galena samples were analysed at Queen's University in Kingston, Canada for $\delta^{34}S$. Table 7, below summarises $\delta^{34}S$ ‰ vs VCDT results.

Table 7. Sulfur isotope composition of galena.

Sample ID	$\delta^{34}S$ ‰ vs VCDT
TS-02	7.2
TS-03	6.9
TS-14	7.3
TS-17	7.4
TS-23	5.3
TS-44	7.3

Standard ID	$\delta^{34}S$ ‰ vs VCDT
NBS123	17.5
IAEA-SO-6	-34.1
NBS127	20.3

Sulfur isotope results gave a narrow range for most samples with an average $\delta^{34}S$ of 6.9‰, with the lowest value being 5.3‰ and the highest 7.4‰.

5.6 Freibergite Geothermometer

The Sack (2005) geothermometry method was used to estimate mineralization temperature at Silver Hart. This method uses ratios of the elements Ag, Cu, Fe, and Zn of galena hosted freibergite inclusions to estimate formation temperatures. $Ag/(Ag+Cu)$ is then plotted on the y-axis against $Zn/(Zn+Fe)$ on the x-axis. This method was originally developed for the Keno Silver District. Table 8, below summarizes temperatures calculated.

Table 8. Mineralization temperatures of freibergite.

Sample	Ag/(Ag+Cu) ap	Zn/(Zn+Fe) ap	Temperature °C	Zone
TS-03_2	0.296	0.447	170	TM
TS-03_3	0.291	0.445	170	TM
TS-03_5	0.303	0.427	170	TM
TS-03_8	0.294	0.452	170	TM
TS-08_1	0.342	0.405	190	TM
TS-08_3	0.344	0.402	190	TM
TS-08_6	0.352	0.453	200	TM
TS-09-2	0.381	0.651	250	TM Wall
TS-09-2-2 (vein in 09-2)	0.517	0.280	250	TM Wall
TS-09-3	0.572	0.311	350	TM Wall
TS-09-4	0.363	0.543	220	TM Wall
TS-09-4-2	0.515	0.548	350	TM Wall
TS-14_3	0.354	0.484	200	S
TS-17-6 inclusion	0.537	0.331	300	M
TS-44_3	0.333	0.339	170	KL

Samples TS-03, TS-08, and TS-44 are from the main TM-K-KL vein zone of Silver Hart, and suggest a temperature of approximately 170-200°C. Sample TS-09 is a piece of wall rock directly adjacent to TS-08, and shows a much more variable temperature of 220-350°C.

6. Discussion

In General, mineralization at Silver Hart is mainly defined by high-grade polymetallic Ag-Pb-Zn veins, with some carbonate replacement style mineralization in areas of limestone. These veins tend to strike NE-SW. Sulfur isotope analysis suggests that magmatic activity was not the sole source of sulfur in the system.

Silver Hart shows many similarities to the Keno Hill Mining district. The host rocks of both are composed of calcareous to epiclastic sediments, breccias, and schists (Boyle 1965). Vein strikes of both areas are roughly NE-SW, and are composed of high grade Ag-Pb-Zn with freibergite being the main silver-bearing mineral (Lynch 1989).

6.1. Mineral and Metal Zoning Patterns

In 2020, a channel sampling campaign was undertaken along the main TM and K vein. Sampling was continuous along the channels, with one meter of rock chips per sample bag perpendicular to the vein strike. The distance between lines of sampling was roughly 20 to 100m. From south-west to north-east, 28 lines of samples were taken on the TM and K zones, resulting in 260 total samples. Figure 20 below, shows sampling locations along TM strike through various bedrock lithologies.

Because of the sampling method, and the very high grade of some of the vein material, sample assay results will vary widely. Some samples may have little to no mineralization, while the ones that are composed of vein material may have several percent lead. However, because this method was used along the entire strike of the TM zone, it would appear useful to determine metal zoning patterns (Pb-Zn, Pb-Ag, Pb-Sb, Cu-Mn).

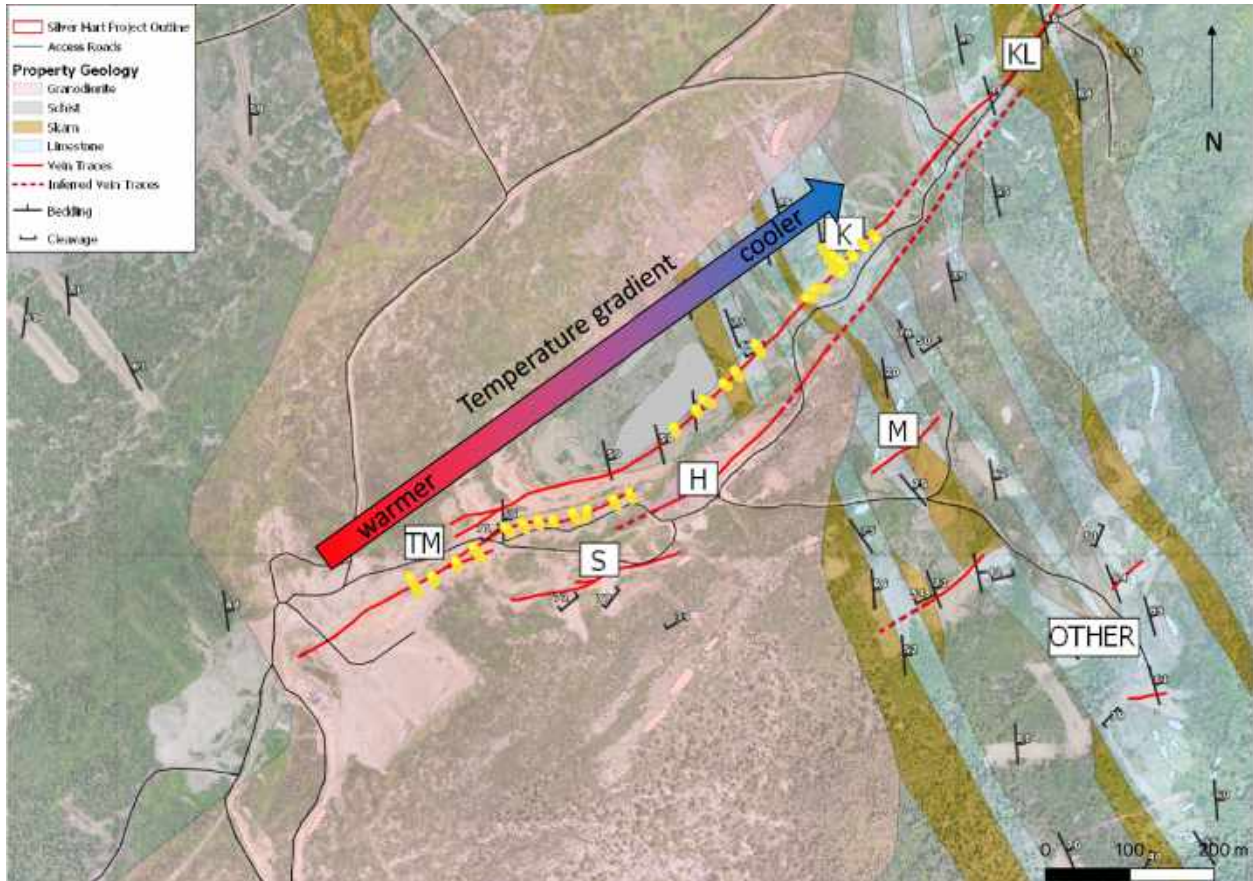
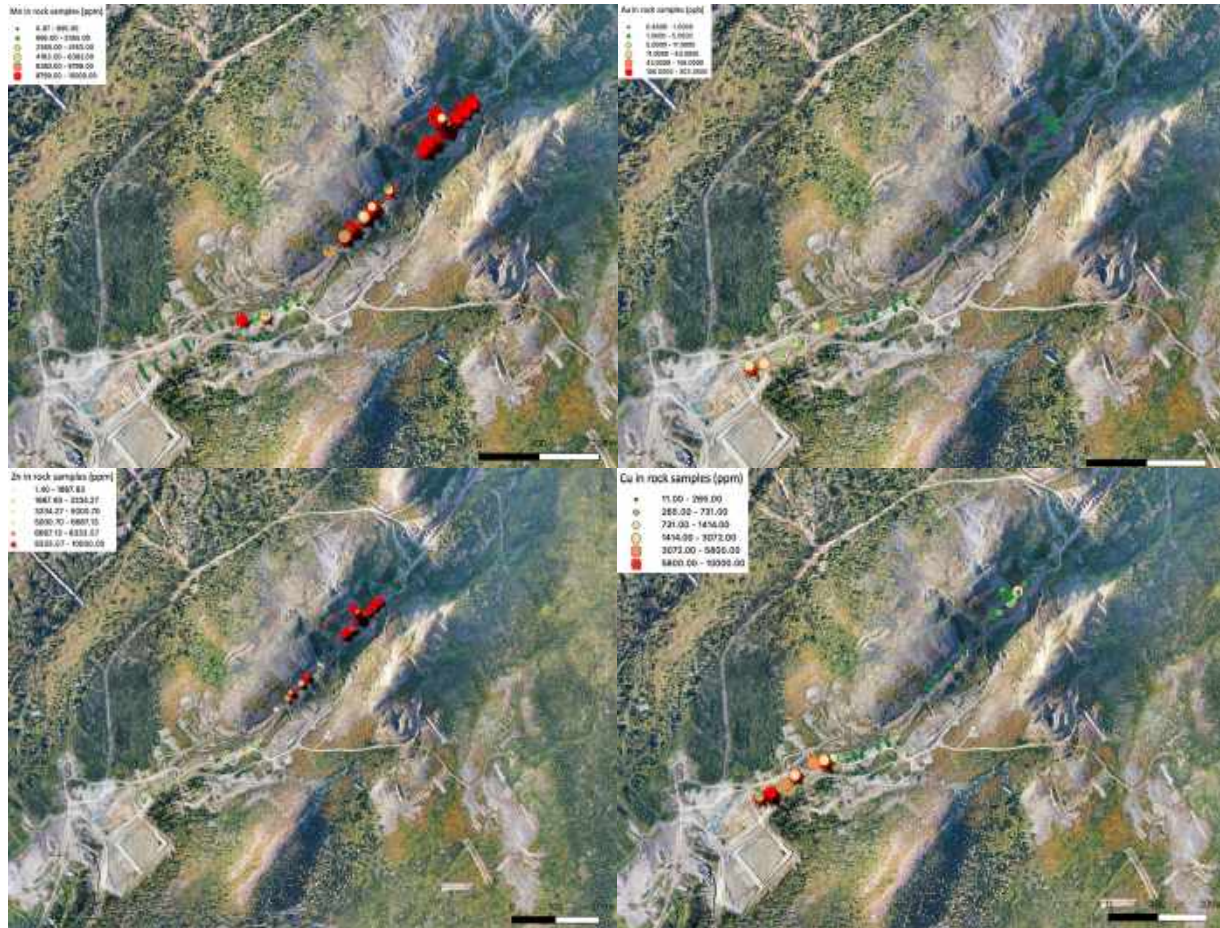


Figure 20, 2020 chip sampling locations along strike of TM vein through 3 different rock types.

With the monzogranite intrusion being a major heat source, elements would be expected to precipitate along a thermal gradient. It is predicted that elements such as copper, gold, and cobalt would occur in higher concentration closer to the intrusion, while elements that precipitate in lower temperature environments such as manganese, zinc, lead, and mercury to occur further away from the heat source. Figures 21 a-d below, show elemental distributions along the TM-K-KL vein structure of manganese, zinc, gold, and copper.



Figures 21 a-d, showing concentrations of manganese (top left), gold (top right), zinc (bottom left), and copper (bottom right) depending on their proximity to an intrusive heat source.

These geochemical maps of elemental distribution do suggest that the lower-left area of the map, representing the TM zone hosts a higher concentration of elements associated with higher formation temperatures. The K and KL zones further to the top right is much richer in manganese and zinc, suggesting a cooler formation temperature, supporting a magmatic-hydrothermal origin of the deposit. In general, the element associations change from Zn-Cu-As-Ag in SW to Zn-Pb-Cu-Sb-Ag-As then Pb-Ag-Sb and finally Pb-Ag in NE.

6.2. Lead Isotopes

In John Bradford’s 1988 thesis, he extensively studied the Rancheria district and its’ silver-lead-zinc deposits. Among the samples he collected were 3 samples from Silver Hart. He concluded that lead isotopes show a mixed fluid source of both magmatic and basinal contributions. Mortensen and Gabites analysed several galena samples from Silver Hart for their 2002 report on lead isotopes in the area. They concluded that the vein and skarn mineralization was biotite schist hosted, of Cambrian age, and sourced from the Cassiar Platform.

6.3. Sulfur isotopes

The positive sulfur isotope composition of galena deviates from typical magmatic sulfur that would be expected to fall around 0 $\delta^{34}\text{S}$ ‰. While purely seawater source sulfate has changed greatly over the last billion years, it is most typically in the range of 15 – 20 $\delta^{34}\text{S}$ (Claypool et al. 1980). With an averaged $\delta^{34}\text{S}$ of 6.9‰ for Silver Hart samples, there is evidence that the sulfur source was not purely magmatic (Shanks 2013).

These results may suggest that there was mixing between hot, low $\delta^{34}\text{S}$ fluid from the Cassiar Batholith intrusion, and cold, high $\delta^{34}\text{S}$ non-magmatic fluid from the sedimentary environment of the Cassiar Platform.

6.4. Silver Mineralogy

Although some silver in galena substituting for lead, it is evident that samples from the main vein zone (TM, K, and KL zones) show strong correlations between silver, copper, and antimony, suggesting these samples (TS-01, 02, 03, 08, 35, 42, and 44) also contain silver-bearing sulfosalts along the strike of the main vein.

Of the 18 samples sent to ALS for assay, TS-02 had by far the highest silver concentrations at 11,050 ppm, with the next highest silver concentration being 7950 ppm for TS-03. This result is unexpected, as TS-03 is entirely massive galena (82.5% Pb), while TS-02 is only 19.15% Pb and galena is much more disseminated. It was hypothesized that silver occurred as inclusions in galena, but this result suggests that there must be another mode of occurrence for silver. TS-02 also had the highest concentrations of copper (17750 ppm), sulfur (20%), antimony (15250 ppm), and zinc (31.4%). The abundance of sphalerite explains the high zinc and sulfur concentrations, while antimony, silver, and copper abundances suggests that there are significant amounts of silver sulfosalts, such as silver-bearing tetrahedrite, pyrargyrite, or freibergite.

Sample TS-17 is massive galena from the M zone. It is characterized by fine grained galena with small inclusions, hosted in limestone. This sample contains the highest lead concentration of all samples assayed at 84.2%, but also the lowest concentrations of copper at only 150 ppm. Despite this, the silver concentration in this sample is 3030 ppm. This would suggest that more than one silver sulfosalt is present on the property. Miargyrite has the formula AgSbS_2 containing equal parts antimony and silver, with no copper. With a silver concentration of 3030 ppm, and an antimony concentration of 3130 ppm, this seems a likely candidate.

Sample TS-23 is from the JD zone, 300m from the M zone. Like TS-17, it is also hosted in limestone, and the outside of the sample reacts strongly with HCl. The silver-antimony ratio of this sample is similar to TS-17 at 1835 and 1150 ppm for silver and antimony respectively. Copper is low at 610 ppm, suggesting that miargyrite (AgSbS_2) or pyrargyrite (Ag_3SbS_3) is also the dominant silver mineral in this sample, and zone.

Accordingly, the geochemical data of vein material indicates that silver occurs in several different minerals. This is supported by the microscopic investigations and SEM results. The identification of these silver-bearing minerals is mainly based on EPMA data which gives the chemical composition of the minerals. These include; freibergite, pyrargyrite, stephanite, diaphorite, and silver-bearing anglesite. The composition of the sulfosalts are illustrated in figure 22 below, which shows a ternary plot of silver-copper-antimony sulfosalts.

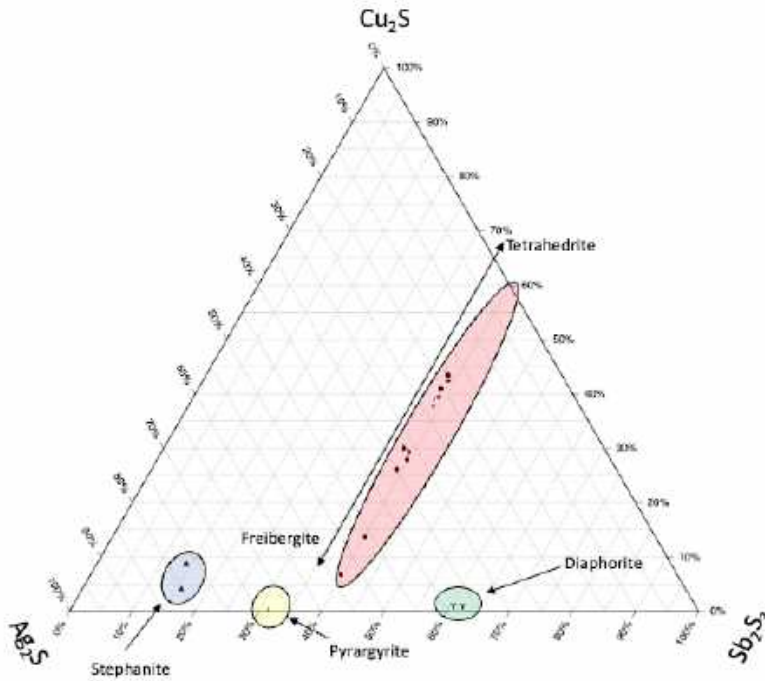


Figure 22. Ag-Cu-Sb ternary plot of sulfosalts in galena.

Because freibergite and tetrahedrite form a solid solution, they tend to plot on a ternary diagram as a line. Antimony and sulfur content remains constant, while silver and copper ratios vary. At Silver Hart, copper and silver ratios in freibergite/tetrahedrite are inversely correlated. We would expect a higher silver to copper ratio indicating cooler areas. There is some evidence to support this, but more sampling along the main TM-K-KL vein is required to confirm or dismiss this theory.

Stephanite ($\text{Ag}_5\text{Sb}_4\text{S}_4$) should plot on this ternary plot at around 80% silver and 20% antimony. It has the right proportions of Ag and Sb, but also contains small amounts of Cu.

Diaphorite ($\text{Ag}_3\text{Pb}_2\text{Sb}_3\text{S}_8$) plots on this ternary diagram where miargyrite (AgSbS_2) should plot, and was initially thought to be miargyrite, however these two samples are the only ones that contain elevated lead, and almost no copper. Table 9, below compares microprobe composition of diaphorite to its theoretical composition.

Table 9. EPMA analytical results vs. theoretical composition of diaphorite in wt%.

Element	Theoretical Composition	TS-44-2A	TS-44-6
Silver	23.8%	23.12%	24.36%
Antimony	26.86%	24.79%	27.89%
Lead	30.48%	32.93%	27.76%
Sulfur	18.87%	18.76%	19.53%

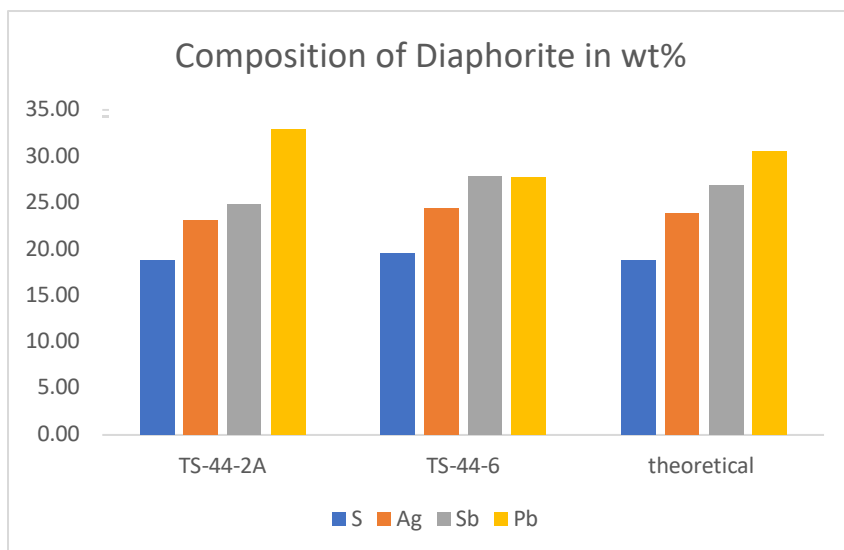


Figure 23. A graphical representation of observed vs. theoretical element Abundances in diaphorite.

Diaphorite was only found in one area, the north-easternmost exposure of galena of the main vein mineralization. This is the KL zone, and is represented by sample TS-44. Hernández and Akasaka (2010) noted that they found diaphorite to be associated with freibergite when $Ag/(Ag+Cu)$ ratio in freibergite was high. They found that the presence of diaphorite with tetrahedrite tended to indicate a crystallization temperature of more than $250^{\circ}C$. They also suggested that diaphorite forms at the expense of galena and freibergite. Sample TS-44 is coarse grained, shows cross-cutting fractures, and evidence of ductile deformation. It is likely that the initial crystallization temperature of freibergite and galena was more than $250^{\circ}C$. Subsequent cooler episodes of mineralization then caused instability, which resulted in the loss of silver from galena and freibergite (Sack 2005). This would suggest that freibergite inclusions which are intersected by a crack or vein could have been affected by a later and lower temperature event, rather than the initial temperature of deposition. The $Ag/(Ag+Cu)$ vs. $Zn/(Zn+Fe)$ ratio calculated in a freibergite crystal from sample TS-44 indicated a crystallization temperature of $\sim 170^{\circ}C$, consistent with a later, lower temperature re-crystallization. This later remineralization would also explain the presence of silver-bearing anglesite ($PbSO_4$) between grains of galena, formed by replacement.

6.5. Geothermometry

Initially, it was planned to use the GGIMF geothermometer in an attempt to determine the temperature of mineralization at Silver Hart. This novel method proposed by Frenzel et al. in 2016 measures the ratios of gallium, germanium, indium, manganese, and iron in grains of sphalerite. They noted that as temperature increases, so does the concentration of manganese, indium, and iron. It also corresponds to a decrease in the concentration of gallium and germanium. This method was attractive as it is especially useful for low temperature SEDEX, MVT and polymetallic vein type deposits up to $310 \pm 50^{\circ}C$ (Frenzel et al. 2016). Electron Probe Microanalysis (EPMA) using Wavelength Dispersal Spectroscopy (WDS) was conducted at GTK in Finland in order to get precise elemental compositions of various minerals in polished pucks.

Unfortunately, of the 26 samples of sphalerite that were analysed, none contained concentrations of all five of the GGIMF elements together in significant enough amounts to be beyond detection limits. For

example, only 2 samples contained indium above detection limits, however these samples were below detection limits for germanium and gallium.

It was further proposed to use the sphalerite-galena geothermometer. This method compares concentrations of cadmium in adjacent grains of sphalerite and galena. While every sphalerite sample was above the detection limit for cadmium (average ~1500ppm with ~430 detection limit), none of the galena samples met the detection limit for cadmium, which was approximately 750ppm.

(Ferrill et al. 2004) suggest that a geothermometry estimation can be made by observing deformation in calcite. Sample TS-26 contains calcite, and the Ferrill et al. technique was used. Twinning is predominately thin, deformed lamellae, suggesting they are type I or type II, meaning that formation temperature was below 250°C.

Using the geothermometry method developed by Sack (2005), 15 freibergite inclusions from 6 galena samples were used to estimate mineralization temperatures. This method is based on ratios of $Ag/(Ag+Cu)$ and $Zn/(Zn+Fe)$ in freibergite. The results are presented in figure 24, below.

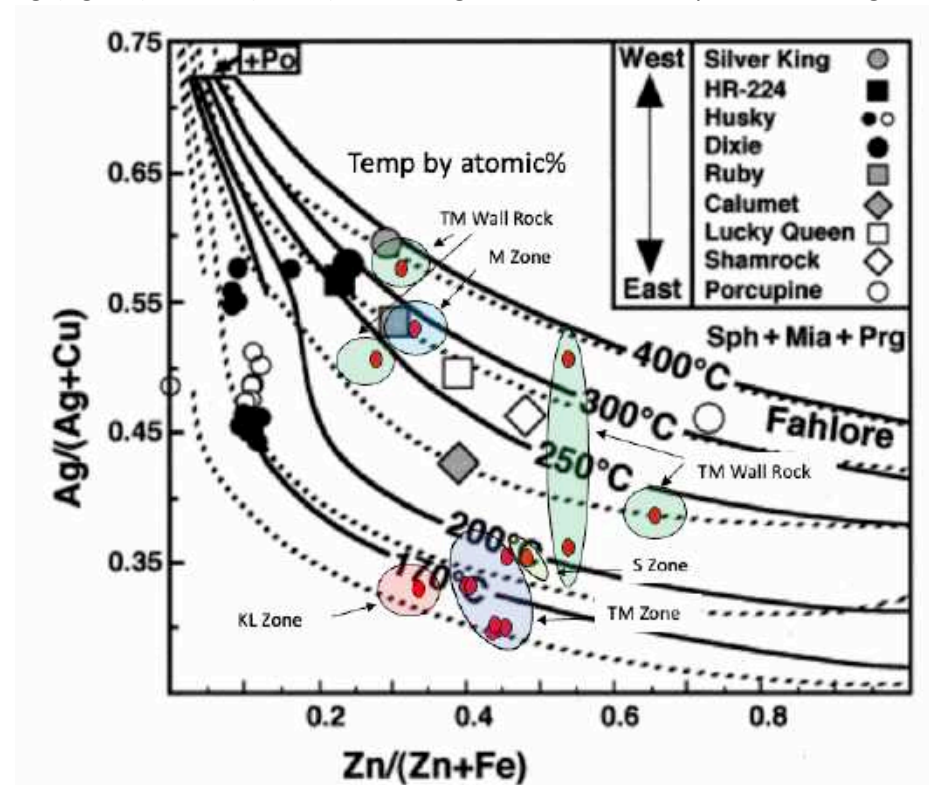


Figure 24. Ratios of $Ag/(Ag+Cu)$ vs. $Zn/(Zn+Fe)$ in freibergite grains from the Silver Hart property (red) highlighted to indicate the zone they were gathered from. Black and white dots are from freibergite grains of the Keno Hill mines (Lynch 1989). Isotherm plot from Sack 2005. Solid lines are original isotherms, while dashed lines are updated isotherms by Sack.

The freibergite grains that were collected from massive galena of the TM and KL main vein zone all plot close to one another in the 170°C - 200°C range.

Sack (2005) notes that in many cases, these mineral assemblage ratios are affected by later remineralization at lower temperatures. The presence of anglesite and diaphorite in Silver Hart galena samples would support this idea. Hernández and Akasaka (2010) found that the presence of freibergite and diaphorite together indicate elevated silver concentrations, and were found when mineralization temperature was above 250°C.

Of the 15 freibergite grains plotted in figure 24, 5 of them are on or above the 250°C isotherm, indicating that some initial mineralization temperatures have been preserved. These are found in the wall rock samples, which may have been protected from later fluid interaction. When all of these factors are taken into account, there is evidence to suggest that the original ore forming fluid temperature was 250°C-350°C. Subsequent cooler mineralization fluids within the veins then leached silver from freibergite which recorded the colder temperature of 170°C-200°C.

7. Conclusion

Based on the results of this thesis, there is strong evidence that the mineral responsible for hosting the majority of silver at Silver Hart is freibergite $(Ag,Cu,Fe)_{12}(Sb,As)_4S_{13}$, a similarity it shares with the Keno City silver district. In the majority of samples sent for bulk assay, silver, copper, and antimony concentrations were strongly correlated. With high copper prices, this adds an attractive extra source of revenue if copper can be recovered. Other minor silver minerals include; stephanite, pyrargyrite, diaphorite, silver-bearing anglesite, and silver substituting for lead in the crystal structure of galena. The average amount of silver in galena strictly due to crystal lattice substitution is 0.15wt%.

Sulfur isotope analyses from 6 pure galena samples gave an average $\delta^{34}S$ of 6.9‰ relative to VCDT, with total range being 5.3 – 7.4‰. This indicates that there was a mixed fluid source from both the Cassiar Batholith intrusion, and basinal brines from the Cassiar Platform.

The vein system records a general metal zoning from SW, where it is hosted by the intrusion, to NE where it extends into metasedimentary rocks. The zoning shows the trend: Zn-Cu-As-Ag – Zn-Pb-Cu-Sb-Ag-As – Pb-Ag-Sb – Pb-Ag, which is likely reflecting a thermal gradient during deposition.

The freibergite geothermometer estimates temperature based on silver-copper, and zinc-iron ratios in freibergite grains. Using this method, two clusters of temperatures emerged. It's likely that the initial mineralizing fluid was 250°C-350°C, recorded in TM zone wall rock, and M zone freibergite. Subsequent cooler mineralizing fluids then remobilised elements, precipitating freibergite with different elemental abundances, and other minerals including diaphorite. This temperature of 170°C-200°C was recorded in freibergite of the main TM-KL vein zone, and in the S zone.

8. References

Abbot, G. 1983. Silver-Bearing Veins and Replacement Deposits of the Rancheria District.

ALS assay laboratories. "2022 fee schedules" <https://www.alsglobal.com/en/geochemistry/geochemistry-fee-schedules>.

Le Bas, M. & STRECKEISEN, A.. (1991). The IUGS systematics of igneous rocks. *Journal of The Geological Society - J GEOL SOC.* 148.

Boyle, R.W (1965). Geology, geochemistry, and origin of the lead-zinc-silver deposits of the keno hill-galena hill area, yukon territory.

Bradford, J.A. (1988). Geology and Genesis of the Midway Silver-Lead-Zinc Deposit, North Central British Columbia.

Claypool, G.E. Holser, W.T. Kaplan, I.R. Sakai, H. and Zak, I. 1980. The age curves of sulfur and oxygen isotopes in marine sulfate and their mutual interpretation. *Chem. Geol.*, 28: 199--260.

Driver, Leslie Ann. Creaser, Robert A. Chacko, Thomas. Erdmer, Philippe; Petrogenesis of the Cretaceous Cassiar batholith, Yukon-British Columbia, Canada: Implications for magmatism in the North American Cordilleran Interior. *GSA Bulletin* 2000;; 112 (7): 1119-1133.

Ferrill, David & Morris, Alan & Evans, Mark & Burkhard, Martin & Groshong, Jr, Richard & Onasch, Charles. (2004). Calcite Twin Morphology: A Low-Temperature Deformation Geothermometer. *Journal of Structural Geology.* 26. 1521-1529.

Frenzel, Max. Hirsch, Tamino. Gutzmer, Jens. Gallium, germanium, indium, and other trace and minor elements in sphalerite as a function of deposit type — A meta-analysis, *Ore Geology Reviews*, Volume 76, 2016, Pages 52-78.

Gabrielse, H. (1985): Major Dextral Transcurrent Displacements along the Northern Rocky Mountain Trench and Related Lineaments in North-central British Columbia. *Geological Society of America, Bulletin*, Vol. 96, pages 1-14.

Gallego Hernández, A.N. and Akasaka, M. (2010), Ag-rich Tetrahedrite in the El Zancudo Deposit, Colombia: Occurrence, Chemical Compositions and Genetic Temperatures. *Resource Geology*, 60: 218-233.

Lynch, J. V. Gregory; Large-scale hydrothermal zoning reflected in the tetrahedrite-freibergite solid solution, Keno Hill Ag-Pb-Zn district, Yukon. *The Canadian Mineralogist* 1989.

Mitchell, G. Mihalynuk, L. and Heaman, L.M. "Age of mineralized porphyry at the logtung deposit W-Mo-Bi-Be (Beryl, Aquamarine), Northwest BC." *British Columbia Geological Survey. Geol. Fieldwork* 1 (2002): 35-40.

Mortensen, J.K. Brand, A. and Liverton, T. 2007. Laser ablation ICP-MS U-Pb zircon ages for Cretaceous plutonic rocks in the Logtung and Thirtymile Range areas of southern Yukon. In: *Yukon Exploration and Geology 2006*, D.S. Emond, L.L. Lewis and L.H. Weston (eds.), Yukon Geological Survey, p. 213-221.

Mortensen, J.K. and Gabites, J.E., 2002. Lead isotopic constraints on the metallogeny of southern Wolf Lake, southeastern Teslin and northern Jennings River map areas, Yukon and British Columbia: Preliminary results. In: *Yukon Exploration and Geology 2001*, D.S. Emond, L.H. Weston and L.L. Lewis (eds.), Exploration and Geological Services Division, Yukon Region, Indian and Northern Affairs Canada, p. 179-188.

Nelson, J. Bradford, J. Geology of the Area Around the Midway Deposit Northern British Columbia. *British Columbia Geological Survey. Geological Fieldwork* 1986, p 186-192.

Dr. Pufahl, Peir. Dr. Leybourne, Matthew & Dr. Layton-Matthews, Daniel. co-Directors QFIR. Queen's University, Facility for Isotopic Research. Private correspondence letter with methods and results of sulfur isotope analyses. Oct 3, 2022.

Roddick, J. A. "Tintina Trench" *The Journal of Geology* 1967 75:1, 23-33.

Sack, Richard O. Internally consistent database for sulfides and sulfosalts in the system Ag₂S-Cu₂S-ZnS-FeS-Sb₂S₃-As₂S₃: Update, *Geochimica et Cosmochimica Acta*, Volume 69, Issue 5, 2005, Pages 1157-1164.

Shanks, Wayne. (2013). Stable Isotope Geochemistry of Mineral Deposits. *Geochemistry of Mineral Deposits. Treatise on Geochemistry*. 13. 59-85.

Sharp, Thomas G. Buseck, Peter R.; The distribution of Ag and Sb in galena: Inclusions versus solid solution. *American Mineralogist* 1993.

Spalla, Maria & Zanon, Davide & Williams, Paul & Gosso, Guido. (2011). Deciphering cryptic P-T-d-t histories in the western Thor-Odin dome, Monashee Mountains, Canadian Cordillera: A key to unravelling pre-Cordilleran tectonic signatures. *Journal of Structural Geology*. 33. 399-421.

Tiljander, Mia. Geological Survey of Finland (GTK). Private correspondence letter with methods and results of microprobe analyses. Aug 16, 2022.

Webster, Ewan R. Archibald, Douglas A. Pattison, David R.M. Pickett, Jessica A. and Jansen, Joel C. Tectonic domains and exhumation history of the Omineca Belt in southeastern British Columbia from ⁴⁰Ar/³⁹Ar thermochronology. *Canadian Journal of Earth Sciences*.

Yukon Geological Survey, 2022. Yukon digital bedrock geology. Yukon Geological Survey, <https://data.geology.gov.yk.ca/Compilation/3>.

9. Appendix

Appendix A. Table of samples

The table below lists all samples collected, and what they were used for.

Table A1. All samples collected from Silver Hart and Blue heaven, detailing what they were used for.

Sample #	Description	Location	Bulk Geochem	Puck Made	Optical Microscope	SEM	Microprobe	Geothermometer	Sulfur Isotope
TS-01	Banded sph and ga	Waste pile, S-W of TM zone	Y	Y	Y	-	-	-	-
TS-02	Banded sph and ga	Waste pile, S-W of TM zone	Y	Y	Y	Y	Y	-	7.2
TS-03	Massive coarse grained ga	southern most pt of TM	Y	Y	Y	Y	Y	Y	6.9
TS-04	TM wall rock (schist)	adjacent to TS-03	-	-	-	-	-	-	-
TS-05	Ox schist w fine sulfides	TM wall rock	-	Y	Y	-	-	-	-
TS-06	Quartz vein	TM wall rock	-	-	-	-	-	-	-
TS-07	Mn stained host rock	TM wall rock	-	-	-	-	-	-	-
TS-08	Ga veinlet fine grained	TM just below H zone	Y	Y	Y	Y	Y	Y	-
TS-09	Py in quartzite	TM just below H zone	-	Y	Y	Y	Y	Y	-
TS-10	fine dis. ga	S-E part of H zone	-	-	-	-	-	-	-
TS-11	Quartzite with chalco	H zone	Y	Y	Y	-	-	-	-
TS-12	black Mn stained rock	H zone	-	-	-	-	-	-	-
TS-13	Mn stained host with dis. ccp, ga, sph	S zone	-	Y	Y	-	-	-	-
TS-14	Fine grained massive ga	S zone	Y	Y	Y	Y	Y	Y	7.3
TS-15	Po bearing qtz breccia	S zone	-	Y	-	-	-	-	-
TS-16	Coarse grained ga	S zone	Y	Y	Y	Y	-	-	-
TS-17	Fine grained massive ga	M zone	Y	Y	Y	Y	Y	Y	7.4
TS-18	Mn stained host of TS-17	M zone	-	-	-	-	-	-	-
TS-19	Mn stained host of TS-17	M zone	-	-	-	-	-	-	-
TS-20	Mn stained host of TS-17	M zone	-	-	-	-	-	-	-
TS-21	Schist host rock	JD zone	-	-	-	-	-	-	-
TS-22	Limestone host rock	JD zone	-	-	-	-	-	-	-
TS-23	Massive med. grained ga	JD zone	Y	Y	Y	Y	Y	-	5.3
TS-24	Calcite w. diss ga and sph	WWM zone	-	Y	Y	Y	Y	-	-
TS-25	Carbonate host rock	WWM zone	-	-	-	-	-	-	-
TS-26	Carbonate fault breccia	WWM zone	-	Y	Y	Y	-	-	-
TS-27	Pyrite in greenstone	WWM zone	-	Y	Y	-	-	-	-
TS-28	Cpy, py, po quartz vein	WWM zone	-	-	-	-	-	-	-
TS-29	Ga and sph vein in qtz breccia	WWM zone	Y	Y	Y	Y	Y	-	-
TS-30	Dis to mass py in greenstone	WWM zone	Y	Y	Y	-	-	-	-
TS-31	Skarn host rock	K zone	-	-	-	-	-	-	-
TS-32	Mn stained breccia	K zone	-	Y	Y	-	-	-	-
TS-33	Skarn host rock	K zone	-	-	-	-	-	-	-
TS-34	Schist host rock	K zone	-	-	-	-	-	-	-
TS-35	Large ga egg	K zone	Y	Y	Y	Y	-	-	-
TS-36	Mn stained schist w. dis ga	K zone	-	Y	Y	-	-	-	-
TS-37	Mn stained schist	K zone	-	-	-	-	-	-	-
TS-38	Qtz breccia with dis sulf	K zone	Y	Y	Y	Y	-	-	-
TS-39	Quartz vein with cc and ccp	K zone	-	Y	Y	-	-	-	-
TS-40	Schist host rock	K zone	-	-	-	-	-	-	-
TS-41	Schist host rock Mn stained	K zone	-	-	-	-	-	-	-
TS-42	Coarse grained ga	K zone	Y	Y	Y	Y	-	-	-
TS-43	Limestone host rock	K zone	-	-	-	-	-	-	-
TS-44	Coarse grained ga	KL zone	Y	Y	Y	Y	Y	Y	7.3
TS-45	monzograinte	T5 drillhole @212m	Y	thin section	Y	Y	-	-	-
TS-46	Biotite schist	T5 drillhole @216m	-	-	-	-	-	-	-
TS-47	Biotite schist	T5 drillhole @199m	-	-	-	-	-	-	-
TS-48	Biotite schist	T5 drillhole @198m	-	thin section	Y	Y	-	-	-
TS-49	Gamet skarn	T5 drillhole @191m	-	Y	Y	-	-	-	-
TS-50	Biotite schist w. qtz and dis sulf	T5 drillhole @184m	-	thin section	Y	Y	-	-	-
TS-51	Fine grained massive ga	Blue Heaven	Y	Y	Y	-	-	-	-
TS-52	Ga veinlets in qtz breccia	Blue Heaven	Y	Y	Y	-	-	-	-
TS-53	Banded sph and ga	Blue Heaven	-	Y	Y	-	-	-	-
TS-54	Skarn host with py and sph	Blue Heaven	-	Y	Y	Y	-	-	-
TS-55	Black host rock, Mn stain	Blue Heaven	-	Y	Y	-	-	-	-
TS-56	Massive med. grained ga (grab samples)	Blue Heaven	-	Y	Y	-	-	-	-

Appendix B. Sample Descriptions

TS-01 This sample is composed of banded sphalerite and galena. Sphalerite occurs as horizontal bands in the layered sample. Galena is disseminated in the sample. At least 4 ore minerals are present, galena, sphalerite, chalcocopyrite, and pyrite. There is evidence of chalcocopyrite disease within sphalerite and chalcocopyrite vein filling in sphalerite. There are small bluish blebby inclusions throughout galena in this sample which will be identified with a SEM. This sample was not picked from bedrock. It was taken from the waste rock pile of a mine adit that was blasted in the 1980's. The layered character of this sample is unique on the Silver Hart property.

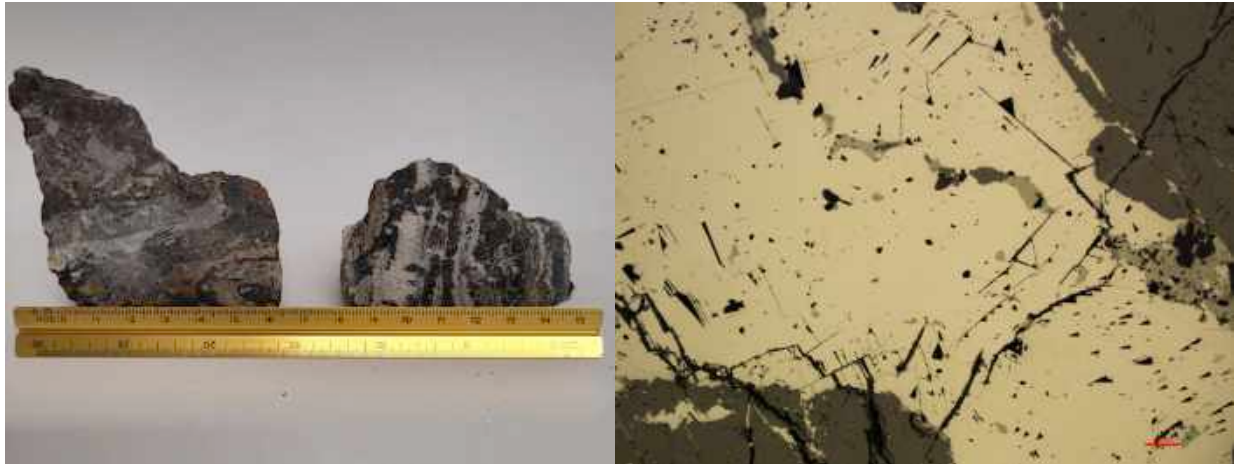


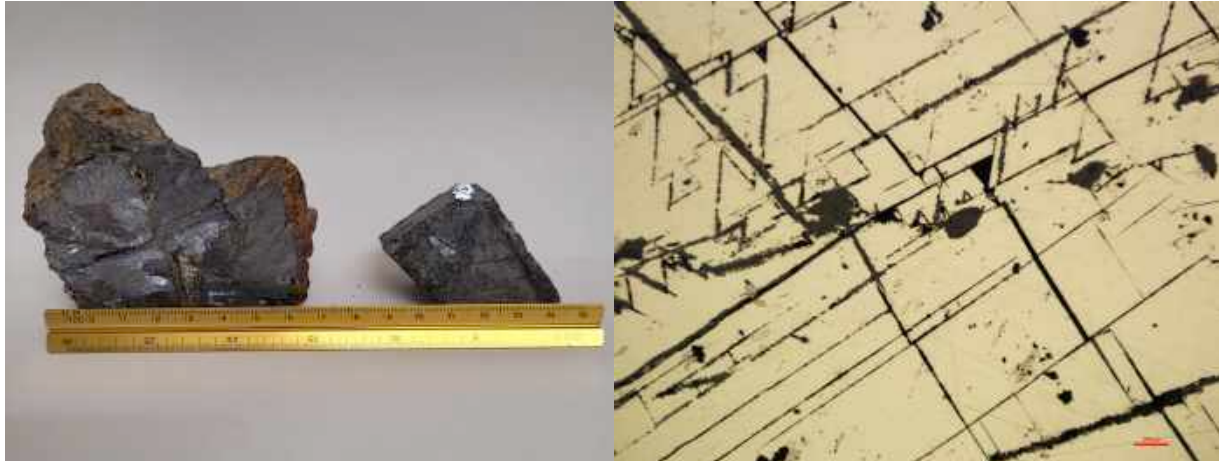
Figure B1 left, and B2 right, showing TS-01 in hand sample and polished puck.

TS-02 This sample is also from the waste rock pile of the now closed mine adit. It is composed of massive galena and sphalerite in alternating bands. Galena grains are euhedral and medium grained. Under the microscope sphalerite is highly fractured, and has mild chalcocopyrite disease. Chalcocopyrite also occurs in fractures of sphalerite. As with TS-01, there are small blebby inclusions in galena.



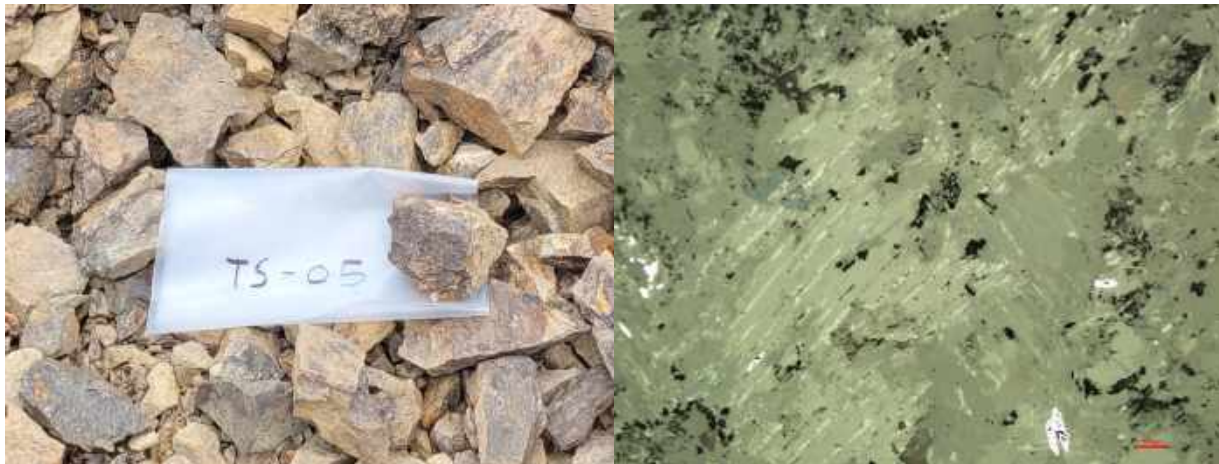
Figure B3 left, and B4 right, is hand sample and polished puck. The polished section shows galena with inclusions, sphalerite with chalcocopyrite disease, and chalcocopyrite filling in cracks.

TS-03 Represents the southernmost exposure of the TM zone. It is composed almost entirely of massive coarse grained galena. There is minor secondary copper alteration in some places and several fractures in the galena. Previous assays by CMC show gold concentrations as high as 300 PPB in this area. Under the microscope, galena is highly fractured with some showing cross-cutting relationships, indicating more than one episode of deformation. Under the microscope, some secondary copper oxidation is visible, as in some occurrences of sphalerite.



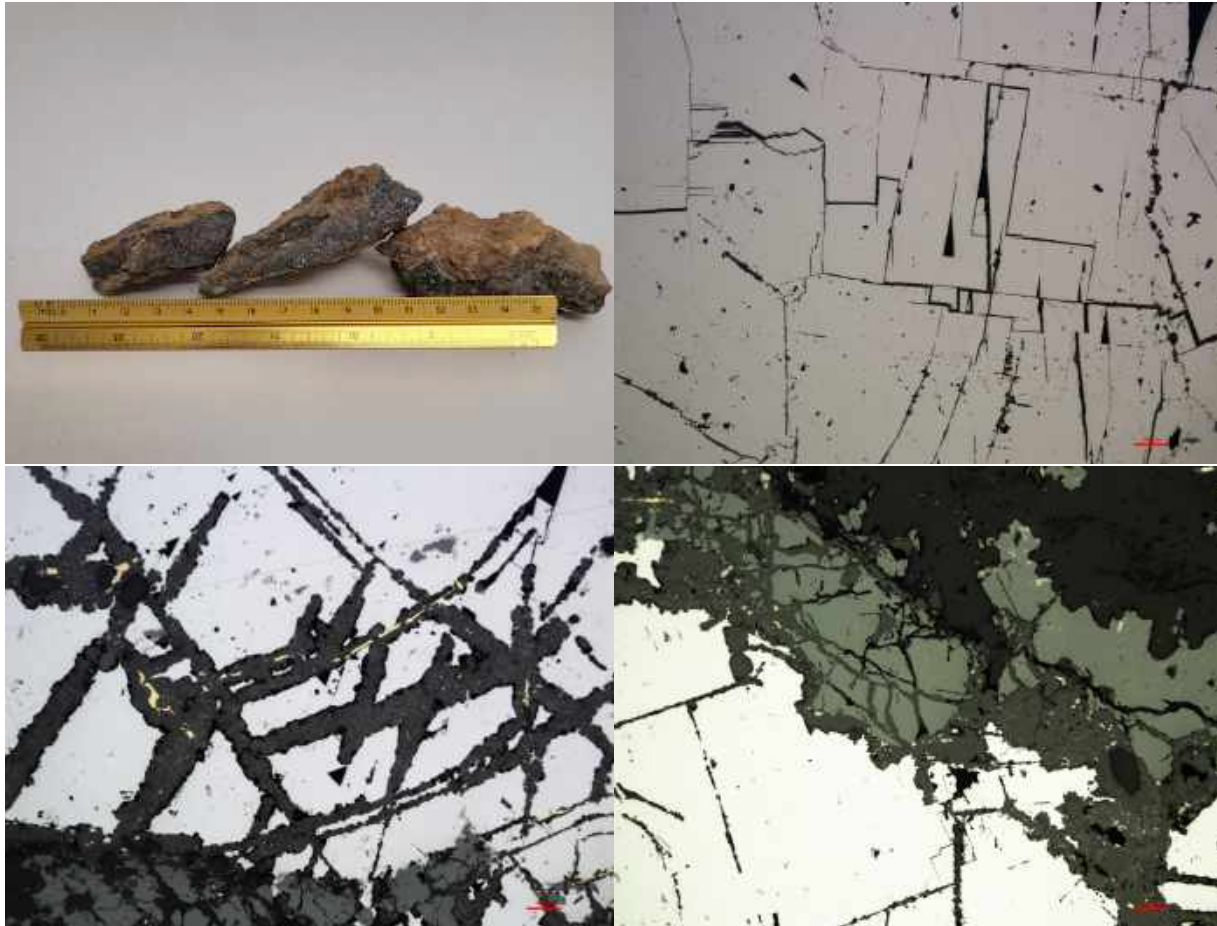
Figures B5 left, and B6 right, Showing hand sample of coarse galena and polished puck of galena with cross-cutting Veins.

TS-05 This is a sample of heavily oxidised schist that was taken from wall rock adjacent to the TM vein. There are finely disseminated sulfides distributed throughout the sample.



Figures B7 left and B8 right, showing TS-05 upon collection (width of ore bag is 30cm), and in polished puck under XPL, with small pyrite Inclusions.

TS-08 While still from the main TM zone, this sample is from a vein slightly northwest of the main TM area. It is characterized by fine grained galena in a vein about 1-2cm thick. Under the microscope, galena grains show evidence of ductile deformation, and some cross cutting relationships in crystal cracks. The galena is highly fractured and filled, partially with chalcopryite.



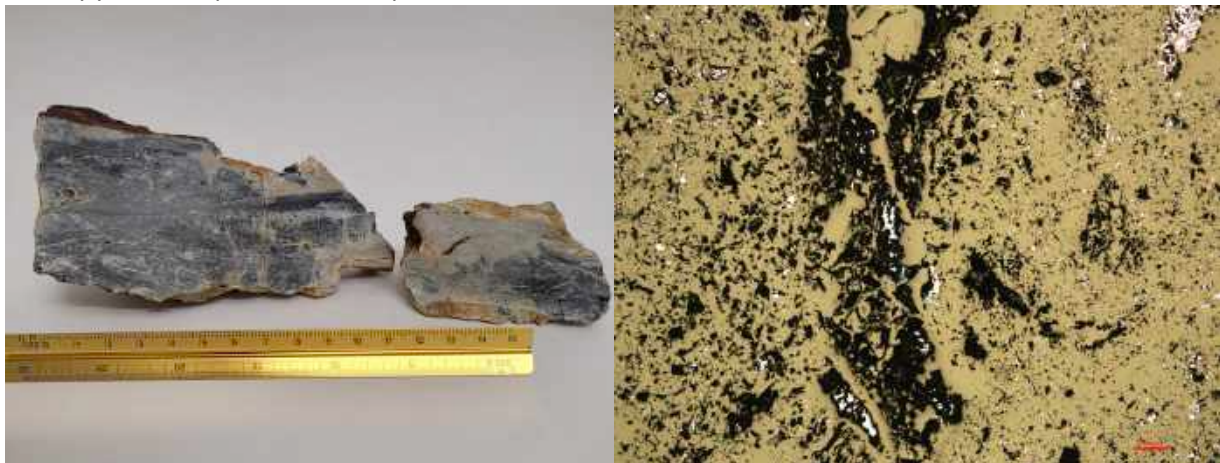
Figures B9, B10, B11, and B12. B9 (top left) showing hand sample of galena. B10 (top right) showing deformation and fracture cross-cutting in galena. B11 (bottom left) showing fracturing and fracture filling with chalcopryite in galena. B12 (bottom right) showing fractured sphalerite with chalcopryite disease, and galena.

TS-09 Contains disseminated sphalerite and pyrite in a quartzite matrix. Pyrite is highly fractured and contains many dark inclusions. It is possible that the inclusions are gangue minerals that have been surrounded by pyrite.



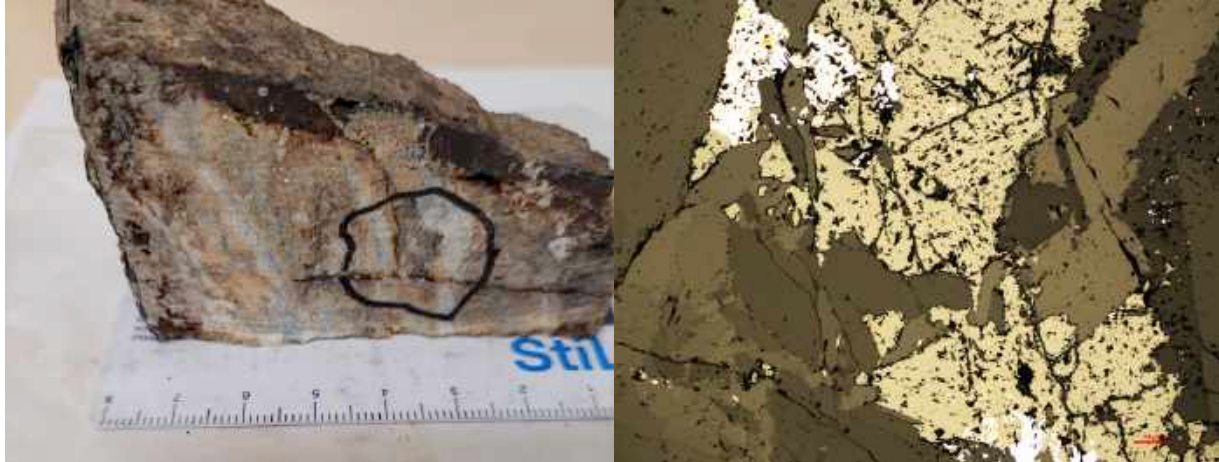
Figures B13 left and B14 right, Showing hand sample (ore bag width is 30cm) and polished section of anhedra pyrite that is highly fractured and hosting many inclusions.

TS-11 Will not be part of this paper. It is composed of quartzite with very minor occurrences of chalcopyrite, and provides no important information.



Figures B15 left, and B16 right, showing hand sample of TS-11 quartzite and polished puck with minor chalcopyrite and chalcocite.

TS-13 This sample is of strongly manganese stained material from southeast of the main TM zone in the S zone. It shows minor galena, sphalerite, and pyrite. Minor chalcopyrite inclusions exist in sphalerite. No previous petrography work has been conducted on material from the S zone.



Figures B17 left, and B18 right. Hand sample identifies where polished puck was cut from. Polished puck shows chalcopyrite (top left), sphalerite (middle), and galena (bottom middle).

TS-14 Represents massive galena from S zone. Galena is fine grained, and occurs with sphalerite. It is cut by veins of quartz and contains sugary quartz inclusions. Under the microscope, galena and sphalerite grains are highly fractured and filled. Wavy patterns within galena shows evidence of ductile deformation.



Figures B19 left, and B20 right. Hand sample shows cut face with fine grained galena and quartz. Polished section shows wavy deformations and triangular pitting in galena.

TS-15 This sample is composed of pyrrhotite bearing material slightly Northeast of sample 14. The cut face shows a conglomerate made of spherical quartz grains cemented together into a type of quartzite breccia. This breccia contains minor amounts of sulfide minerals, likely pyrrhotite or pyrite.



Figure B21, hand sample showing cut face in TS-15.

TS-16 Is composed of massive vein style galena mineralization. This may represent the true S zone East of the H zone. The galena grains are coarse and look to be deformed in hand specimen. There are small subparallel veinlets of quartz and pyrite throughout the sample. Under the microscope, it is evident that galena is heavily deformed. We can see evidence of at least 2 stages of deformation. Cross-cutting relationships and displacement of several large veins are visible. The contact with quartz is very sharp, with little to no transition zone from quartz to galena.



Figures B22 left, and B23 right. Hand sample of galena and polished puck showing deformation and pitting of galena crystals.

TS-17 This sample is from the M zone. This area is marked to be just within the carbonate belt the runs East-West across Silver Hart and is characterized by intense manganese staining. In hand sample, the galena is very fine grained and massive. Mild iron staining, likely oxide or hydroxide occurs within galena. Under the microscope minor non-ore minerals, likely quartz are evenly distributed throughout the sample. The galena is very competent and shows very little fracturing. There are abundant small blebby blue inclusions. Potentially these are silver minerals that appear to have a defined lineation within the sample. A large filled fracture shows evidence of displacement across it.



Figure B24 (left) Showing hand sample of massive fine-grained galena, and B25 (right) showing light blue inclusions in galena.

TS-23 Is the furthest east sample of the Silver Hart property. It is located within the limestone belt and represents carbonate replacement galena. The galena grains in this sample are medium grained and do not show the euhedral crystal character of many other samples. Fine veinlets of gangue minerals are pervasive. The outside of the sample is highly vesicular and reacts strongly with hydrochloric acid. In polished section, regular cleavage breaks in galena are visible, as are odd irregular grain boundaries. The texture suggests that fine, rounded grains were fused together creating large galena crystals with remnants of past grain boundaries.



Figures B26 left, and B27 right. Hand sample showing cut face of massive galena. Figure Y shows straight cleavage fractures, and remnants of rounded mineral grains.

TS-24 Was taken from the so-called WWM trench. This is an under-explored area slightly North of the KW zone. This sample contains euhedral calcite and some finely disseminated sphalerite. There is strong oxidation on the outside of the sample. Under the microscope, we can identify at least 4 different sulfide minerals; galena, sphalerite, pyrite, chalcopyrite. The sphalerite contains chalcopyrite in several areas and may have chalcopyrite disease. The boundary between sphalerite and galena is sharp and smooth. Pyrite occurs as sharp, euhedral crystals, suggesting that they are late-stage formed and are not deformed.



Figure B28 left, showing freshly collected hand sample (bag width 30cm). Figure B29 right, showing galena (left), sphalerite with chalcopyrite disease (centre), and euhedral pyrite (right).

TS-26 Is a piece of carbonate breccia. There is fault slickensides on one side of the sample, suggesting that this sample is fault gouge composed of carbonate breccia. In polished section, twinning in calcite is very apparent. Twinning is predominately thin, deformed lamellae, suggesting they are type I or type II, meaning that formation temperature was below 250°C (Ferrill et al. 2004). There is also a high-relief mineral phenocryst containing abundant euhedral pyrite.





Figures B30, B31, and B32. Figure B30 showing hand sample collection (bag width 30cm). Note slickensides on rock to the top left of frame. Figure B31 (right) showing twinning present in calcite grains. Figure B32, of a phenocryst rich in pyrite grains. Minor chalcopyrite is also present in the top left of frame.

TS-27 Contains abundant disseminated pyrite in a foliated greenstone matrix. The greenstone is weakly reactive to HCl. Pyrite appears to also follow some kind of lineation. In polished section, pyrite grains are subhedral to euhedral, and contain abundant inclusions. Minor chalcopyrite is present in some areas.



Figure B33 left, showing freshly collected sample (ore bag width 30cm). Figure B34 right, showing euhedral to subhedral pyrite with inclusions. Minor chalcopyrite is visible just above scale bar.

TS-29 Is from the bottom of a trench in the WWM zone. It is not certain that this sample is from outcrop, but was taken from a very large rock exposure that is likely bedrock. The hand specimen shows disseminated to vein mineralization of galena and sphalerite in a brecciated matrix. In polished section, cross-cutting relationships are visible in galena. Many fractures in galena and sphalerite are filled with chalcopyrite. Grey blebs, potentially some kind of silver mineral are prevalent in galena. They occur as circular to oblong, bluish-grey inclusions that in some areas may constitute up to 5% in galena. Chalcopyrite occurs mainly as a vein filler in sphalerite or at galena-sphalerite boundaries.

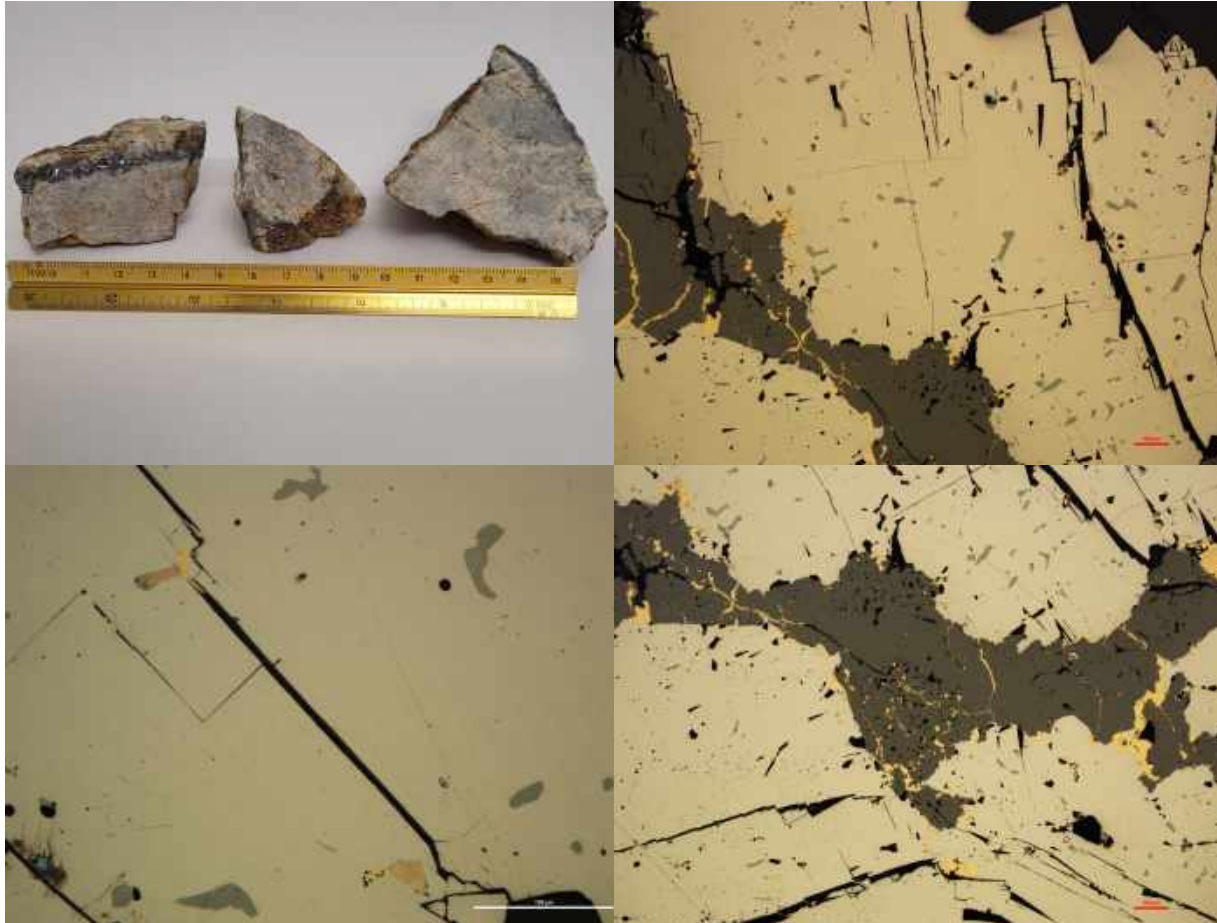


Figure B35, top left showing the hand sample with a vein of galena. Figure B36, top right showing galena with blebby inclusions, and sphalerite with chalcopyrite vein filling. Figure B37, lower left shows displacement of a fracture, plus several galena inclusions of chalcopyrite and a yet to be identified grey-blue mineral. Figure B38, lower right shows galena with abundant inclusions, and sphalerite with chalcopyrite filling voids and fractures.

TS-30 Shows strong disseminated pyrite mineralization in non-carbonate schist. The hand specimen is slightly green in colour. The pyrite appears to follow the general foliation fabric of the host rock. In polished section, pyrite occurs as anhedral grains that have been rounded and contain abundant inclusions.



Figure B39 left, showing disseminated to massive laminated pyrite and B40 right, showing anhedral pyrite grains in polished puck.

TS-32 Was originally thought to be a sample of massive sphalerite, but has since been reclassified as a sample of strongly stained breccia. Under the microscope, some small (<10 μ m) euhedral pyrite grains occur. They occur exclusively in a dark mineral, and may have exsolved from it and recrystallized. Minor disseminated chalcopyrite is also present in this sample.

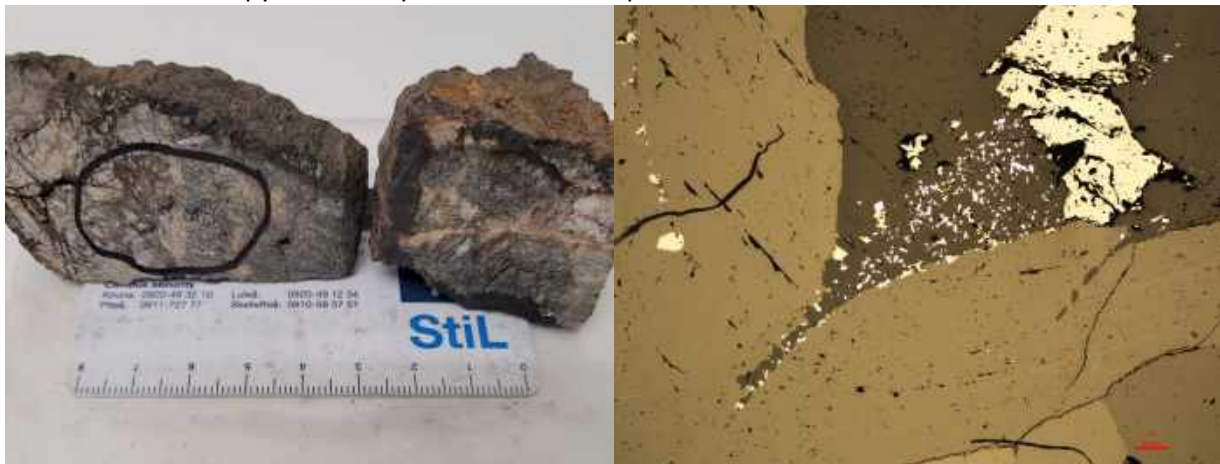


Figure B41 left, showing cut face of sample and area polished puck was cut from. Figure B42 right, showing euhedral pyrite grains and inclusion rich sphalerite in an unknown dark mineral.

TS-35 Is from the K vein zone. This unique sample, a galena 'egg' occurs as a an approximately 2.5cm thick shell of galena surrounding a circular core of gangue mineral. The core rock is strongly altered at the edges and contains minor disseminated pyrite. The galena surrounding the core is euhedral, in some cases showing perfectly formed crystals. The galena-gangue contact is roughly 1mm thick and is highly porous and contains iron hydroxide.



Figure B43, galena egg hand sample. A small piece of the core is visible in right sample just above the ruler.

TS-36 This sample is composed of disseminated sulfides in a schist matrix. Isolated euhedral sulfides are present.

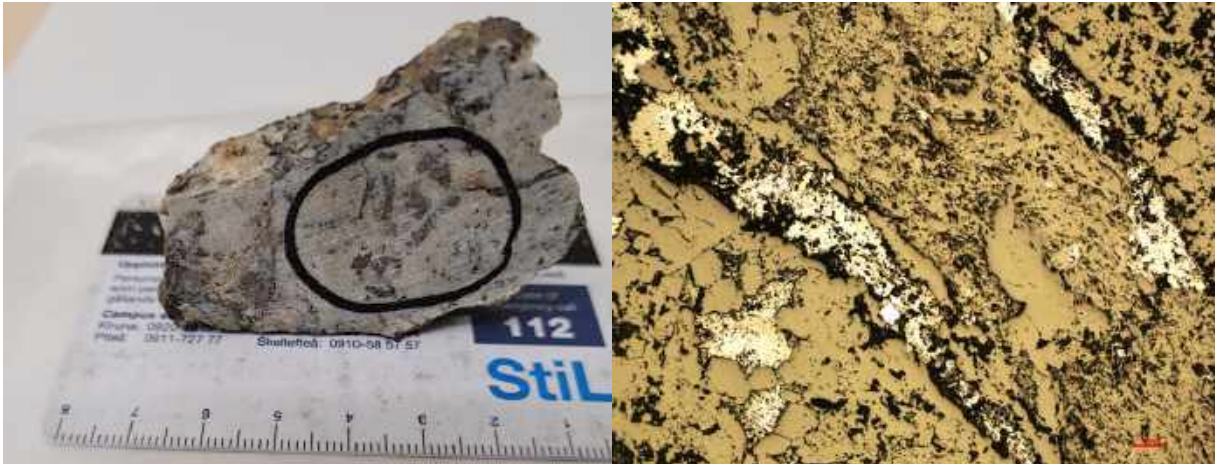


Figure B44 left, and B45 right. Hand sample showing area puck was cut from. Polished puck right, shows a single euhedral pyrite grain in matrix (centre of field of view).

TS-38 Is not vein material, but was taken from an area close to the K zone. The matrix is composed of quartz breccia and it hosts disseminated pyrite and sphalerite. Pyrite occurs as fine grained euhedral crystals distributed throughout the sample, while sphalerite occurs as large (100-500 μ m) amorphous grains. Sphalerite has many inclusions as well as chalcopyrite disease.



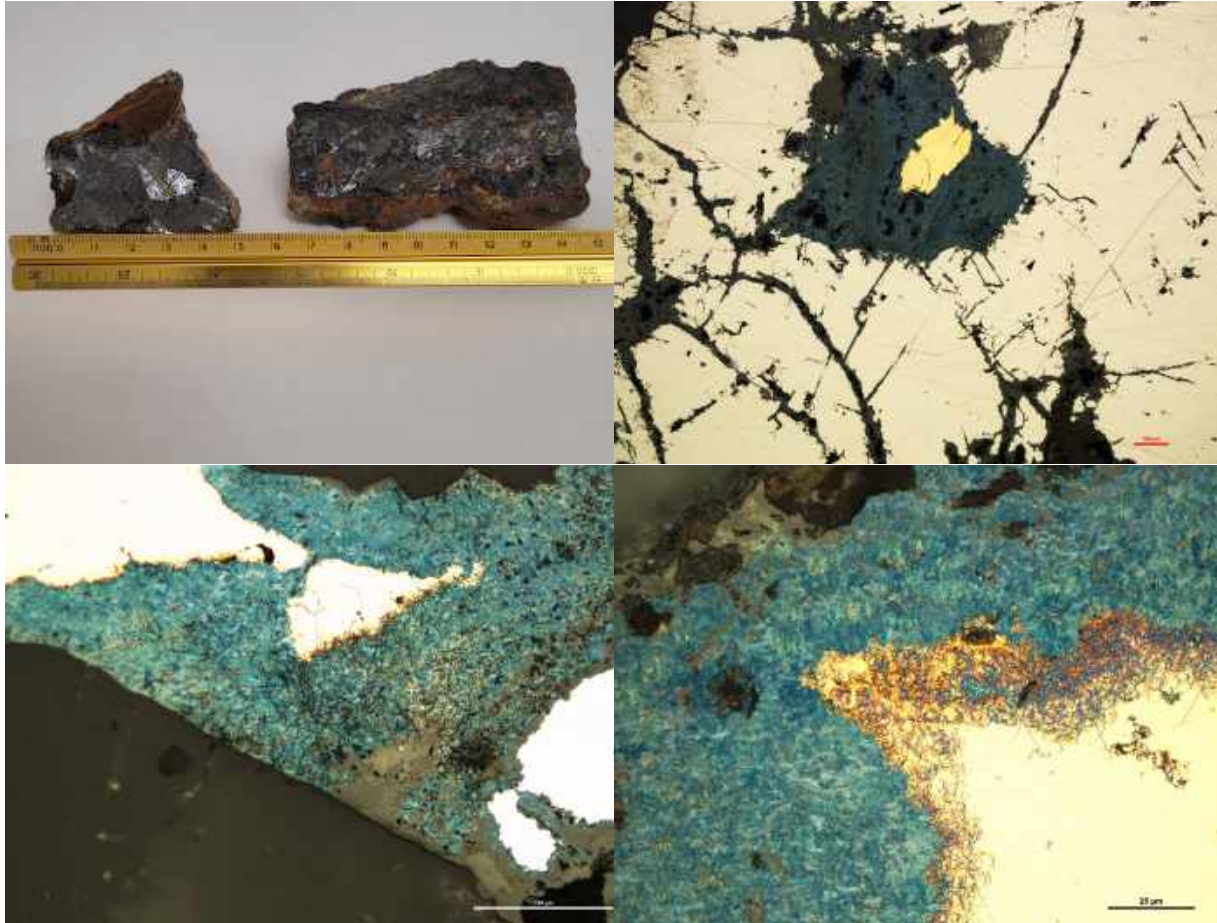
Figure B46 left, showing brecciated hand sample on cut face. Figure B47 right, Showing inclusion rich sphalerite with chalcopyrite disease, and euhedral pyrite grains.

TS-39 Is a sample of a quartz vein that was located within, and parallel to the K zone vein. The only mineralization present in this sample is a small single grain of chalcopyrite and chalcocite.



Figure B48 left, of quartz hand sample on cut face. Figure B49 right, showing a single grain of chalcopyrite and chalcocite in quartz.

TS-42 This is a sample from the K zone where it crosses into the limestone lithology. It is composed of massive galena. There is iron hydroxide and blue copper staining on the outside of the sample. On the cut face, galena is coarse-grained and massive. Some blue copper staining exists on the inside of the sample, along with a chalky yellow mineral, which is likely scorodite. In polished section, the blue mineral is likely chalcocite, which occurs with chalcopyrite, filling cracks and spaces in galena. The transition zone from chalcopyrite to chalcocite has an odd fibrous texture that resembles curly hairs. In some areas, this texture continues into the chalcocite.



Figures B50, B51, B52, and B53. Figure B51, top left, shows hand sample of TS-42 along cut face with prevalent iron hydroxide staining. Figure B52, top right, shows irregularly fractured and filled galena. Many of the fractures are filled with chalcocite. Figure B53, bottom left, Shows bladed black filaments within chalcocite. Figure B54, bottom right shows a circular swirly fibrous texture in the transition zone from chalcopyrite to chalcocite, and within the chalcocite.

TS-44 This is the northernmost exposure of vein type galena on the Silver Hart property. It is part of the KL zone, which may be a continuation of the TM zone. This sample is composed of massive coarse-grained galena with iron hydroxide staining on the outside of the sample. Inclusions of pyrite and scorodite are present, as are thin gangue veinlets. Some copper staining is present on the exterior and cut surfaces of the hand samples. In polished sample, there is evidence of at least 2 deformation events. Many of the older fractures are filled with a dark mineral with a dull lustre. Certain parts of this mineral have colour changing characteristics. Several subhedral galena grains are surrounded by a bluish-grey halo of a different mineral. When this halo is observed under a microscope, it rapidly changes colour from bluish-grey to black. The higher the magnification used, the faster this change occurs. In one area, changing colour completely in less than 2 minutes. Small circular black dots begin to appear in the blue-grey mineral. More and more of these circles appear until the entire mineral has changed. This change is likely caused by heat or light from the microscope, and the change is permanent. Figures B57 and B58 below show this rapid colour change. The time elapsed between taking each photo is 2 minutes. Figure B57 shows the change already occurring before the first photo could be taken.

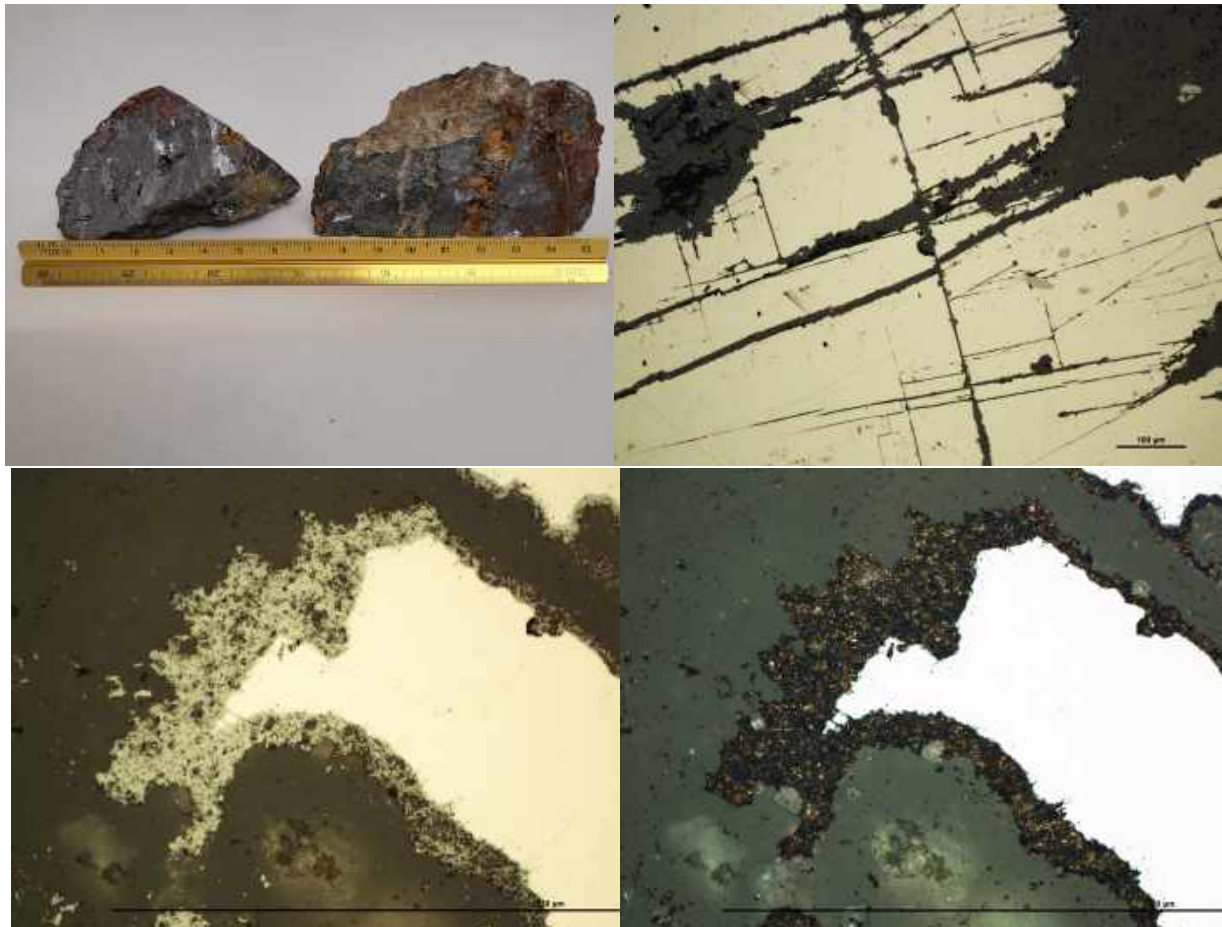


Figure B55, top left, showing hydroxide stained hand sample with scorodite and pyrite. Figure B56, top right, shows cross cutting fractures in galena grains. Larger fractures are filled with blue and black sugary material. Figure B57, bottom left. Time = 0 minutes, change already taking place, and figure B58, bottom left, after 2 minutes at 50X magnification.

TS-45 This is a sample of the monzogranite intrusion. It was taken from the T5 drillhole located at 405274, 6690030. It is from 212.45-212.80m of depth. It is composed of X Y and Z.



Figure B58, monzogranite intrusion of the Cassiar batholith.

TS-49 This sample was taken from the T5 drillhole, located at 405274, 6690030. It is composed of garnet skarn and was from 190.75-190.95m of depth. There are very minor occurrences of pyrite or pyrrhotite, otherwise the sample is completely gangue material.



Figure B59 left of garnet skarn. Figure B60, right showing a small piece of pyrrhotite in reflected light.

TS-51 Is galena from the adjacent Blue Heaven property. It is composed of massive fine-grained galena with disseminated pyrite. Iron hydroxide is prevalent around the outside of the sample. Under the microscope, this sample is highly fractured and deformed. Fracture filling of chalcopyrite in sphalerite is common. This sample also has small inclusions of the mineral from TS-44 that changes colour under the microscope.



Figure B61 left, showing hand sample on cut face. Figure B62 right, of fractured galena with inclusions, sphalerite with inclusions and chalcopyrite.

TS-52 Is composed of massive to veinlet stringers of fine-grained galena within a quartz breccia matrix. Some chalky yellow mineral, likely scorodite is also present in this sample from Blue Heaven. In the polished sample, the galena is very strongly fractured, and filled with a gangue mineral, likely quartz. Some blebby inclusions of chalcopyrite and sphalerite are present in galena grains.



Figure B63 left, of sample showing cut face. Figure B64 left, of cubically fractured and filled galena grains.

TS-53 Is a sample of banded sphalerite and galena from the same vein as TS-52, but taken further North. The polished puck shows highly fractured ore minerals. There is a boundary between galena and another sulfide mineral, likely chalcopyrite that seems to show one mineral overprinting another. Fine-grained euhedral pyrite is also present in this sample.



Figure B65 left, showing hand sample and surrounding rocks (ore bag width 30cm). Figure B66 right, showing galena (centre), chalcopyrite (centre-left), and euhedral pyrite grains (far left).

TS-54 Contains layered bands of very fine-grained galena and fine-grained sphalerite, in a skarn matrix. In the polished puck, the sample has a strange fingerprint like texture. The sphalerite has been fractured along the same plane in many different places and then filled with a gangue mineral, leaving a texture that looks like the rock was stretched open and the gaps filled. Much of the sphalerite has chalcopyrite disease, and minor chalcopyrite filling in some fractures. Subhedral to euhedral pyrite grains with abundant inclusions are present in this sample.

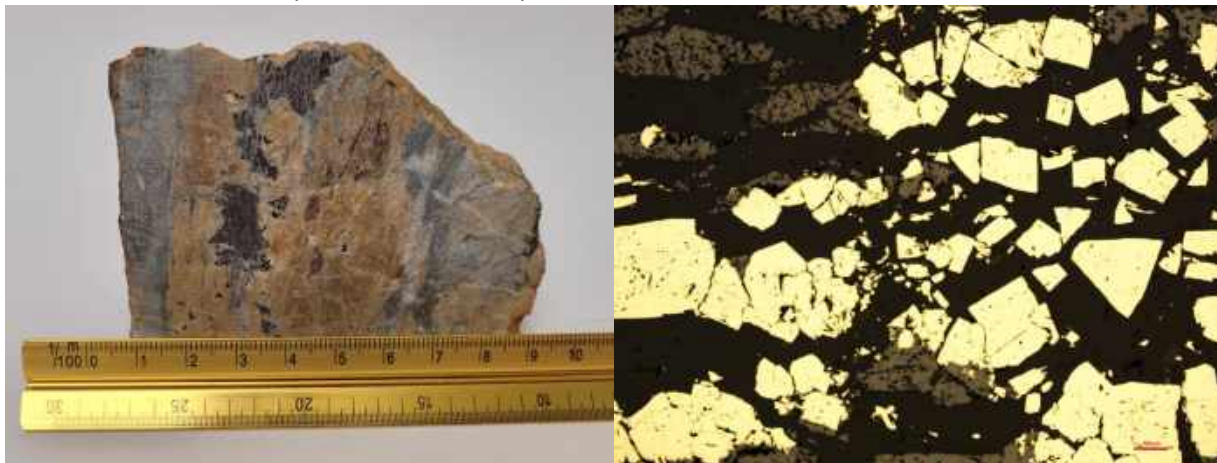


Figure B67 left, hand sample showing cut face. There is a band of sphalerite from cm 2.5 to cm 4, and a band of fine grained galena from cm 6-7. Figure B68 right, polished section showing fractured sphalerite (left) and euhedral pyrite growth (right).

TS-55 This is a very strongly manganese stained rock. It is completely black in colour with some streaks of rusty red chalky minerals. This sample is very porous, and readily absorbs liquids dropped onto it. Some larger pore spaces have long, thin bladed crystals growing within them. The puck was able to be polished, but it is very difficult to identify any minerals present in this sample due to intense alteration.



Figure B69 left, showing the intense dark staining throughout this sample. Figure B70 right, showing heavily altered wavy textures.

TS-56 This sample was not extracted from an outcrop, but was rather a grab sample from a large pile of rock on the ground. Since the exact source of this sample cannot be determined, it will not be used in this study. This sample is fine grained massive galena with hydroxide staining around the outside. The cut face shows that the sample is made up entirely of galena with small vesicles but no other minerals are visible. There appears to be a lineation present in the galena, giving a wavy texture to the sample. In polished section, cross-cutting relationships can be seen in several fractures, with the older and newer fractures hosting different minerals.



Figure B71 left, Showing cut face of galena with a slight tiger stripe pattern. Figure B72 right, showing cross cutting veins in galena.